

# Integrated Functionality of Photothermal Hydrogels and Membranes in Solar Water, Chemical, Mechanical, and Electrical Domains

Wei Li Ong, Wanheng Lu, Tianxi Zhang, and Ghim Wei Ho\*

Solar energy can be harnessed and converted into heat via the photothermal effect, which can then be utilized to drive many other reactions to produce important resources, such as water, fuel, electricity, and even mechanical actuation in a clean and sustainable manner. Hydrogels and membranes coupled with photothermal materials are particularly suitable for this purpose because they possess advantageous properties, such as porosity and adaptability. These properties allow for the introduction of diverse additives and functionalities, ensuring that photothermal systems can be customized for specific tasks, thereby enhancing their overall performance, functionality and versatility. This review aims to provide an overview of recent developments and the significance of employing photothermal hydrogels and membranes in multiple fields ranging from clean water, fuel production, electricity generation to mechanical actuation, followed by a discussion on key considerations in materials design and engineering. Finally, the review addresses the challenges and future directions of photothermal applications.

released as phonons (heat) via a relaxation process.<sup>[1,2]</sup> This photothermal heat can then be used to produce many other essential resources such as electricity, water, green fuel, and even mechanical actuation in a clean and sustainable way. One ideal candidate for this photo-to-thermal “converter” is photothermal hydrogel and membrane, due to their advantageous properties such as porosity and flexibility, which enhance the versatility, scalability, and compatibility of photothermal technology. Unlike photovoltaic devices, these specially designed hydrogels and membranes convert light energy into heat energy, which is then utilized by thermoelectric generators or thermogalvanic cells to produce electricity.<sup>[3,4]</sup> Additionally, hydrogels can be designed with photoactive

materials that absorb solar irradiation to produce electrons and holes, which then participate in redox reactions with the aqueous environment to produce solar fuels such as hydrogen gas and hydrocarbons.<sup>[5,6]</sup> The porous networks and hydrophilic nature of these hydrogels and membranes can also aid in the production of clean water via solar steam generation and photothermal membrane distillation.<sup>[7,8]</sup> Moreover, hydrogels and membranes can be designed using thermo-responsive polymers or materials with different thermal expansion to produce light-powered actuators.<sup>[9,10]</sup>

In the following sections, we will present a broad overview of the photothermal effect, followed by a discussion on the significance of photothermal hydrogels and membranes in advanced engineering applications, together with materials design and engineering. The versatility across multiple fields ranging from clean water, fuel production, electricity generation to mechanical actuation will then be described and discussed. Finally, the challenges and future directions of photothermal applications will be provided to conclude this review (Scheme 1).

## 2. Integrating the Photothermal Technology with Hydrogels and Membranes for Versatile Engineering Applications

Photothermal conversion technology finds diverse engineering applications, such as solar energy harvesting, water purification, seawater desalination, catalysis, environmental remediation, and medical treatments/devices.<sup>[11–20]</sup> Among these

## 1. Introduction

In today's world of high energy demands and depleting natural resources, renewable energy sources, such as solar, wind and tidal, are increasingly being harnessed to meet our needs. Among these, solar energy presents as the most abundant renewable energy source. This immensely powerful energy can be tapped to produce other important forms of energy such as electricity, typically accomplished with photovoltaic cells. However, in recent years, many researchers have reported the conversion of light into heat via the photothermal effect, where photons (light) are absorbed through an excitation process and subsequently

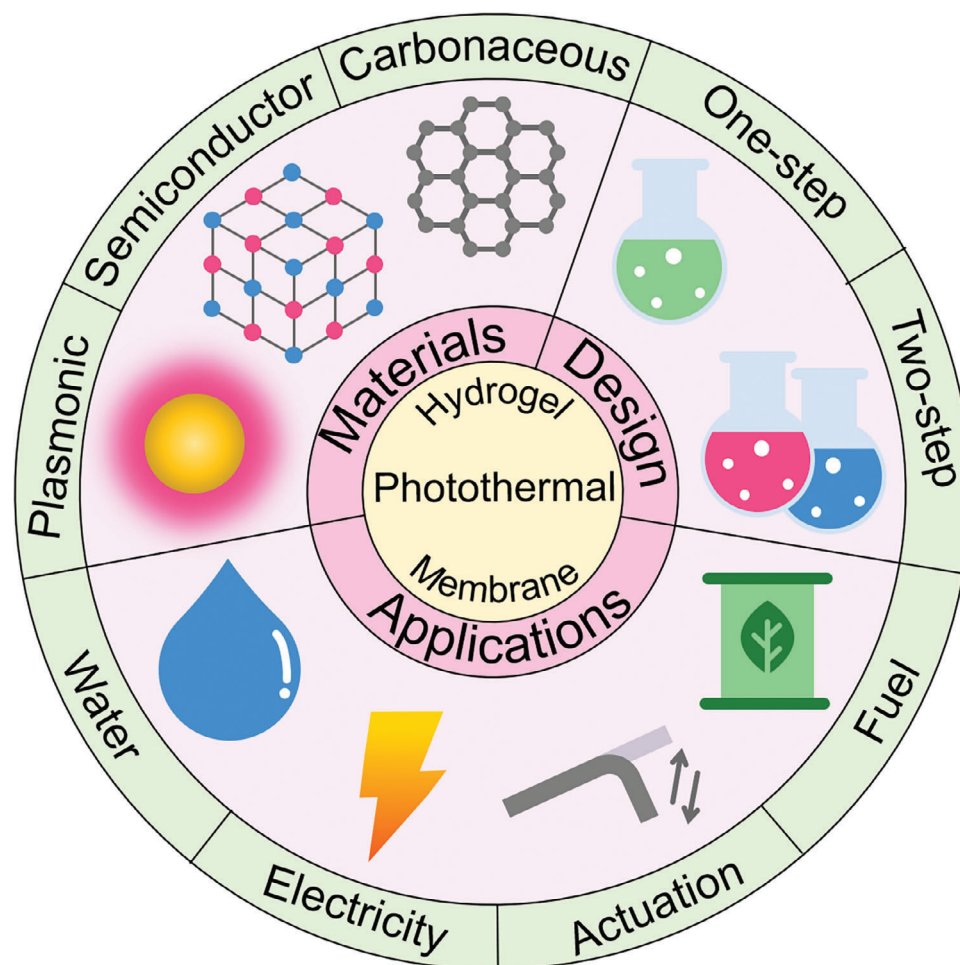
W. L. Ong, W. Lu, T. Zhang, G. W. Ho  
Department of Electrical and Computer Engineering  
National University of Singapore  
4 Engineering Drive 3, Singapore 117583, Singapore  
E-mail: elehwg@nus.edu.sg

G. W. Ho  
Department of Materials Science and Engineering  
National University of Singapore  
9 Engineering Drive 1, Singapore 117575, Singapore

G. W. Ho  
Institute of Materials Research and Engineering  
A\*STAR (Agency for Science, Technology and Research)  
3 Research Link, Singapore 117602, Singapore

The ORCID identification number(s) for the author(s) of this article can be found under <https://doi.org/10.1002/admt.202401110>

DOI: 10.1002/admt.202401110



**Scheme 1.** Overview of photothermal hydrogels and membranes [www.flaticon.com](http://www.flaticon.com).

applications, photothermal technology often takes the form of hydrogels and membranes.<sup>[21–26]</sup> These forms of photothermal hydrogel/membrane enhance versatility, scalability, and compatibility, while imparting unique characteristics inherent to hydrogels and membranes. This is crucial for effective implementation of photothermal technology in engineering applications. To delve deeper into hydrogel- and membrane-hosted photothermal technology and its future development, this section will explore motivations for adopting these forms and their associated benefits. Definitions and basic characteristics of hydrogels and membranes will be introduced, followed by discussions on their unique features when integrated with photothermal technology. Finally, the resulting benefits and potential promises will be explored.

## 2.1. Basic Characteristics of Hydrogels and Membranes

### 2.1.1. Hydrogels

Hydrogels are three-dimensional networks of cross-linked hydrophilic polymeric chains, known for their high water retainability, soft and flexible nature, nontoxicity, biocompatibility, and

extensive tunability in structures and properties (**Figure 1a**).<sup>[27–30]</sup> The high water retention capability of hydrogels lays a foundation for their applications in biological research, water treatment, energy generation and storage. Typically, hydrogels can retain water amounting to 70% to  $\approx 100\%$  of their total weight within their 3D networks, maintaining a solid or quasi-solid form without any water leakage.<sup>[31–34]</sup> In some cases, such as superabsorbent hydrogels, the water retainability can reach up to thousands times their weight.<sup>[35,36]</sup> The soft and flexible nature of hydrogels, coupled with their nontoxic chemical composition akin to living organisms, make them stand out as the optimal materials for biological research and the advancement of soft electronics in the booming field of human–machine interface.<sup>[37–40]</sup> The structures and properties of hydrogels are influenced by numerous factors, including polymer composition, crosslinking density, water content, additives and reinforcements, and network structures.<sup>[27,41,42]</sup> By adjusting these parameters, either individually or in combination, hydrogels can be tailored to exhibit distinctive characteristics: porous versus dense,<sup>[43,44]</sup> soft versus stiff,<sup>[45]</sup> stretchable versus rigid,<sup>[46]</sup> conductive versus insulating,<sup>[47]</sup> charged versus neutral,<sup>[48]</sup> and stimuli-responsive versus nonresponsive.<sup>[49–51]</sup> This highlights the extensive tunability of hydrogels for a wide range of applications.

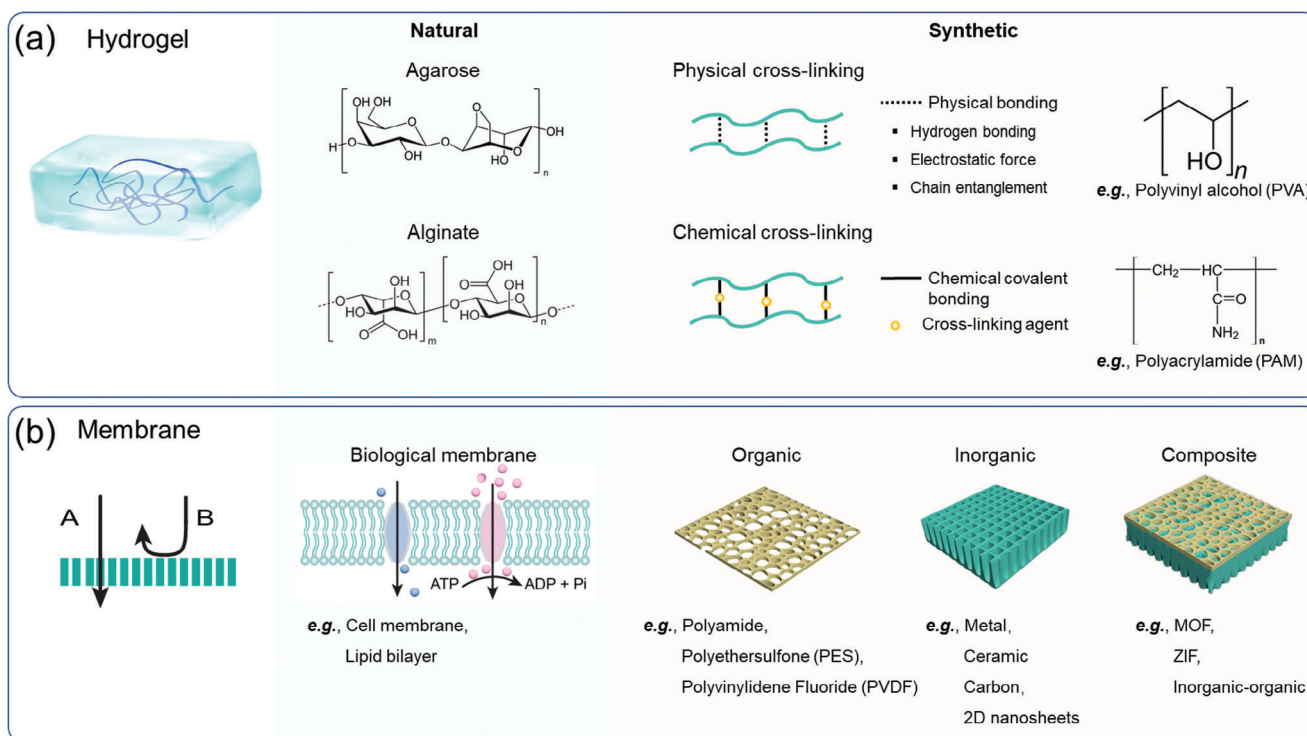


**Figure 1.** Schematic illustration of the typical structural moieties and compositions of a) hydrogels and b) membranes.

In terms of fabrication, hydrogels offer great diversity, accessibility, and scalability. A wide selection of materials and methods can be used to prepare various types of hydrogels in a straightforward and scalable manner. Based on the raw materials, hydrogels can be classified into natural and synthetic. Typical natural hydrogels, such as agarose, alginate, gelatine, and chitosan are widely used in applications like food, cosmetics, biological research and medical applications.<sup>[52–55]</sup> A large family of synthetic hydrogels, such as polyacrylamide (PAM), polyvinyl alcohol (PVA), polyacrylic acid (PAA), and poly(N-isopropylacrylamide) (PNIPAM), can be readily obtained via physical or chemical cross-linking.<sup>[48,56–59]</sup> Moreover, hydrogels can serve as a compatible platform for designing functional materials. Various components, ranging from 0D nanoparticles,<sup>[25,60]</sup> 1D nanofibers or nanotubes,<sup>[61]</sup> and 2D nanosheets<sup>[62,63]</sup> to materials beyond the nanoscale,<sup>[24]</sup> can be readily incorporated to enhance or tailor hydrogels with desired features. The ability to adapt to existing continuous manufacturing processes and scale up materials fabrication is essential for practical engineering applications. Hydrogels offer this advantage in large-scale production, as many hydrogel fabrication methods can be adapted to continuous manufacturing processes, such as extrusion,<sup>[64]</sup> casting,<sup>[65]</sup> electro-/chemical spinning/spray,<sup>[66,67]</sup> 3D printing,<sup>[68]</sup> and even 4D printing.<sup>[69,70]</sup>

In practical applications, photothermal hydrogels can be used in the form of bulk hydrogels,<sup>[71]</sup> hydrogel films,<sup>[72]</sup> and even microgels<sup>[73]</sup> depending on the specific application. For solar water evaporation and chemical (e.g., hydrogen generation and CO<sub>2</sub> reduction) applications, the hydrogels are usually in the form of bulk or film due to advantages such as uniform distribution of catalysts and ease of material recovery and recycling. Having a film morphology will enable the hydrogel to float at the air–water

interface for optimal water evaporation performance with minimal heat loss. There is also usually a high water content in the hydrogel because the water within hydrogel networks has a lower enthalpy of evaporation compared to bulk water, hence, producing a higher rate of evaporation. Moreover, the water stored in the hydrogel can also serve as a water reservoir for photocatalytic water splitting. Microgels are seldom used for solar water evaporation and chemical production because of the difficulty in recovery and recycling of the photothermal microgels compared to bulk or film hydrogels. However, microgels are commonly used in biomedical applications such as drug delivery and photothermal therapy. As for electricity generation and mechanical actuator, bulk and film hydrogels are also preferred as thermoelectric and thermogalvanic cells might require the hydrogel to be flexible and in conformal contact with the surface of interest, while hydrovoltaic and osmotic energy conversion require the hydrogel to be in a planar form for optimal water flow and ion transport. In these cases, the presence of water in the hydrogel is mainly to facilitate the movement of ions and flow of water to generate an electrical output. For mechanical actuation, the hydrogel needs to bend and actuate, hence flexible films will be more ideal. In this case, water content in the hydrogel is not crucial, but thermo-response is important because most photothermal actuators employ PNIPAM hydrogels that actuate in response to temperature changes.

### 2.1.2. Membranes

A membrane is a selective barrier that permits certain substances to pass through while blocking others, depending on the size,

shape, charge, or chemical affinity (Figure 1b). This selective permeability, or the ability to selectively control and manipulate mass transfer at a molecular level, is central to the characteristics of membranes and membrane processes, which enables efficient separation of specific components from mixtures. Without membranes, some separation processes may become highly energy-consuming or even impossible.<sup>[74,75]</sup> Additionally, membranes often operate as a compatible and compact module within systems, allowing for easy and space-efficient integration into various applications. Given their simplicity in configuration and operation, membranes do not require specialized knowledge or attention for their effective use.

Like hydrogels, membranes can be classified as natural and synthetic membranes. Natural membranes are commonly found in living organisms, where they selectively allow the passage of substances and facilitate metabolic processes in biological systems.<sup>[76]</sup> Based on the materials used for construction, synthetic membranes can be further categorized into organic, inorganic, and composite membranes. These types of membranes are commonly used in a range of applications, including purification and separation, catalysis, sensing, and energy generation and storage.<sup>[77–82]</sup> As mentioned, the pore geometry (size, size distribution, and shape) and surface properties (charge and chemical affinity) are key factors determining the nature and performance of membranes.<sup>[83–86]</sup> These factors can be tuned during or after the membrane fabrication process. By employing different fabrication methods or adjusting fabrication parameters, such as reaction temperature and time or introducing additives, membranes with varying pore structures and surface properties can be produced.<sup>[87–89]</sup> Additionally, membrane features can be modified in a post-fabrication approach.<sup>[90,91]</sup> For smart and stimuli-responsive membranes, such as those incorporating stimuli-responsive components, the post-fabrication modifications can be reversibly adjusted with external stimuli.<sup>[92,93]</sup> Conventional membrane fabrication methods include the phase inversion technique,<sup>[94]</sup> interfacial polymerization,<sup>[95]</sup> layer-to-layer assembly,<sup>[96]</sup> electrospinning,<sup>[97]</sup> sol-gel technique,<sup>[98]</sup> extrusion,<sup>[99]</sup> coating,<sup>[100]</sup> self-assembly,<sup>[101]</sup> and also 3D printing.<sup>[102]</sup> Recent emerging methods include 2D nanosheet stacking<sup>[103]</sup> and air/liquid-interface-constrained membrane growth.<sup>[104]</sup> The 2D nanosheet stacking method leverages abundant interlayer spaces as nanoscale channels to control mass transfer. Air/liquid-interface-constrained membrane growth facilitates the large-scale production of free-standing inorganic membranes, overcoming notorious long-standing challenges in the development of inorganic membranes as most of the traditional methods are catered for preparation of organic membrane. Both conventional and emerging membrane fabrication methods can produce membranes with desired features on a large scale for various engineering applications.

To briefly summarize, this section has highlighted the unique properties of hydrogels and membranes that make them indispensable in many applications. Both hydrogels and membranes exhibit high feasibility, flexibility, and scalability in terms of design, functionality, and fabrication. These characteristics are of great significance for practical engineering applications. Photothermal materials can be easily incorporated into hydrogels and membranes to create photothermal-

integrated systems, which retain the advantageous properties of the original hydrogels or membranes. In the next section, the effects of the photothermal incorporation on the integrated hydrogel or membrane will be discussed, whereby the resulting new features and potentials will be summarized.

## 2.2. Advantages and Potentials of the Photothermal-Hydrogels/Membranes Integration

Integrating photothermal technology into hydrogels and membranes creates a mutually beneficial situation. The mutual benefits are schematically shown in Figure 2c, where hydrogels and membranes offer an ideal platform for incorporating photothermal technology with enhanced photothermal effect, robust bonding, and localized heating, while the addition of photothermal materials endows the original hydrogel or membrane systems with new functionalities including solar energy harvesting, noninvasive and precise light control, and reaction facilitation.

### 2.2.1. Hydrogels/Membranes as Ideal Supporting Materials for Photothermal Materials

The structural characteristics of hydrogels and membranes, particularly their high porosity, in addition to their compatibility with additives, make them ideal platforms for hosting photothermal nanomaterials. The porous structure typical of most hydrogels and membranes not only provides a large surface area for accommodating photothermal materials but also improves light absorption for enhanced photo-to-heat conversion by trapping light more effectively (Figure 2c(i)).<sup>[105,106]</sup> In these confined spaces, photothermal materials come into close contact with the absorbed substance molecules (e.g., water), effectively improving heating efficiency by increasing heat conduction and reducing heat loss to the environment (Figure 2c(ii)). Moreover, the flexibility of hydrogels and membranes in material selection and surface property modification allows for the formation of strong bonds between photothermal materials and the hydrogels or membranes, effectively anchoring the photothermal materials within the system (Figure 2c(iii)). Compared with the photothermal materials dispersed in solutions, these strong bonds prevent the loss of photothermal materials, thereby extending their operational lifespan.

Besides hydrogels and membranes, various conventional materials such as polymers, ceramics, and glass<sup>[107–109]</sup> are commonly used as supporting matrices for hosting photothermal materials. However, compared to these conventional materials, hydrogel and membranes offer distinct advantages in the distribution of photothermal materials, light absorption, heat management, and property tunability. First, photothermal materials can be easily incorporated into precursors or directly assembled into hydrogels or membranes using various manufacturing techniques (as detailed in Section 3), allowing for high loading capacity and uniform distribution. In contrast, incorporating photothermal materials into ceramics and glass is more challenging, as it typically requires high-temperature melting or sintering

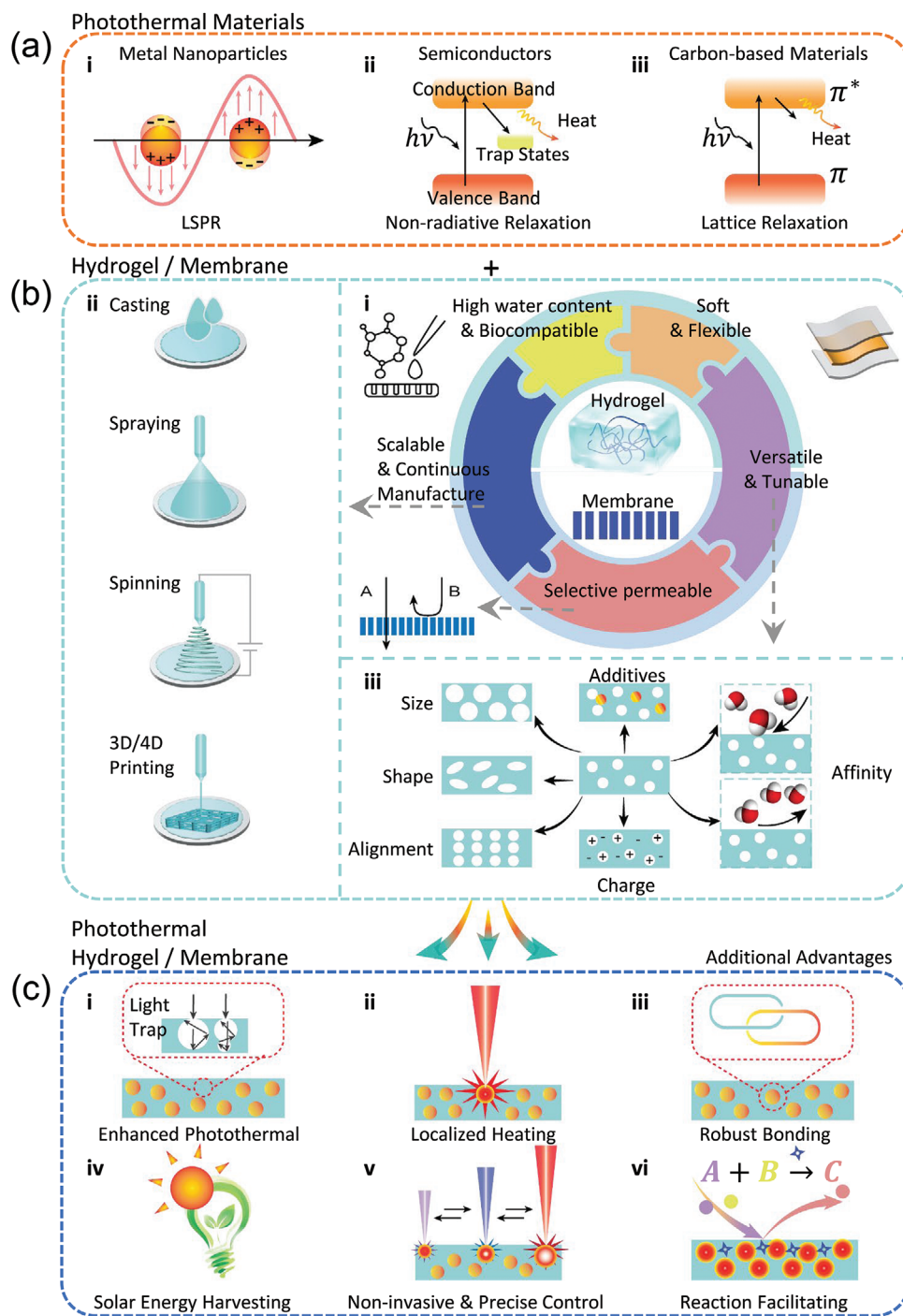


**Figure 2.** Overview of photothermal materials, and their combination with hydrogels or membranes, forming photothermal hydrogels or membranes. a) Typical photothermal materials and mechanisms underlying the photo-to-thermal conversion. b) Unique characteristics of hydrogels and membranes. c) Features of photothermal hydrogels or membranes.

processes to embed and distribute the materials.<sup>[110]</sup> Second, hydrogels and membranes generally feature porous structures ranging from the micro- to the nanoscale, and even down to the sub-nanoscale. These porous structures can enhance light absorption and provide large surface areas for direct and localized interaction between water (or other sub-

stances) and the photothermal materials, thereby shortening the mass and heat transfer paths. As a result, incorporating photothermal materials into hydrogels or membranes significantly enhances the photothermal effect. Third, conventional materials often exhibit rigidity in both mechanical and functional properties, making them less adaptable or flexible for

certain applications, such as biological systems or smart channels. Hydrogels, however, can be engineered with mechanical properties that mimic biological tissues, such as elasticity and flexibility, enabling their use in unique biological applications. Additionally, hydrogels and membranes can be easily customized with specific properties to meet various needs, such as stimuli-responsive behavior for smart channels. These photothermal hydrogels and membranes have already demonstrated their potential in applications such as light-controlled thermotherapy, drug releases, and fluidic control.<sup>[111–113]</sup>

### 2.2.2. Photothermal Materials-Instilled New Features in Hydrogels/Membranes

On the other hand, incorporating photothermal materials also introduces new features to the original systems, enabling hydrogels and membranes to harness solar energy, provide localized heating, offer noninvasive and precise stimuli control, and facilitate chemical reactions. Such advantages can significantly accelerate advancements in various fields, including water desalination and purification as well as green and blue energy generation, and many more.

**Solar Energy Harvesting:** The most evident advantage of incorporating photothermal materials into hydrogels and membranes is their ability to harness renewable and abundant solar energy (Figure 2c(iv)). Solar light is captured by the photothermal materials and converted into heat, which is then transferred to the hydrogel or membrane to activate new functionalities. For example, both hydrogels and membranes are used in water desalination and purification. By incorporating photothermal materials, solar energy can be harnessed to drive the water desalination processes, leading to the development of solar-driven water evaporation<sup>[114]</sup> or solar-driven membrane distillation.<sup>[21,115]</sup> Similarly, in the field of atmospheric water harvesting (AWH), the addition of photothermal materials has led to the development of a new technology known as solar-driven AWH.<sup>[116,117]</sup> Beyond water treatment, the porous structure and customizable surface properties of hydrogels and membranes enable the generation of electricity through mechanisms such as liquid streaming<sup>[118]</sup> and salinity gradient (also known as blue energy).<sup>[119]</sup> Integrating photothermal materials can enhance electrical output by utilizing solar energy to provide heat to sustain liquid flow, maintain moisture gradients, or control ion diffusion.

**Localized Heating and Its Noninvasive and Precise Control:** Compared with bulk heating equipment, photothermal materials can provide localized heating at micro- and even nano-scale under light illumination (Figure 2c(v)). Light is a noninvasive stimulus that can be precisely controlled in terms of its characteristics (e.g., wavelength and intensity) as well as its spatial and temporal resolution. Therefore, integrating photothermal materials into hydrogels and membranes can enable light-controlled remote localized heating.

**Facilitate Chemical Reactions:** Photothermal materials encompass a broad family of materials, including metal nanoparticles, carbon materials, and semiconductors. The photo-to-heat conversion processes in these materials often generate charges,

like hot electrons or electron–hole pairs. These charges, along with the generated heat, can facilitate chemical reactions within the hydrogel or membrane system (Figure 2c(vi)).<sup>[120,121]</sup> Moreover, some photothermal materials have antibacterial properties, enhancing their applications in water purification.<sup>[122]</sup>

### 2.2.3. Distinction Between Photothermal Hydrogels and Membranes

In the previous discussion, we broadly explored the basic characteristics and unique features that arise from incorporating photothermal materials into hydrogels and membranes. In this section, we will examine the distinctions between photothermal hydrogels and photothermal membranes, along with their specific applications. Before proceeding further, it is important to clarify that hydrogels and membranes are not strictly distinct from one another. Hydrogels are a type of material that is soft, flexible, and have chemical and physical properties similar to biological tissues; whereas membranes are more application- or function-oriented and best described as a material-enabled process designed for selective mass permeability (Figure 2b(i)). This means that hydrogels can be used as a material for synthesizing membranes when designed for membrane processes. Given that photothermal materials in applications are commonly used in the forms of hydrogels and membranes, discussions in this paper are divided into photothermal hydrogels and photothermal membranes.

As discussed in Section 2.1, hydrogels and membranes share common characteristics such as flexibility in manufacturing and versatility in modifying their properties and structures (Figure 2b(ii,iii)), however, they differ significantly in structure (though both of them have porous structures) and properties, particularly when tailored for specific applications.

Hydrogels are three-dimensional, water-swollen networks capable of holding large amounts of water, making them soft, flexible, and similar to biological tissues. The interconnected pores within these 3D networks enable efficient incorporation of photothermal materials and enhance heat and mass exchange between the water, photothermal materials, and the surrounding environment. Photothermal hydrogels are widely used in biological applications where chemical and mechanical compliance are critical, such as light-controlled biomedical devices for drug release, tissue engineering, and wound sensors.<sup>[112,123,124]</sup> Additionally, the water within hydrogel networks exhibits a lower enthalpy of evaporation compared to bulk water. Therefore, when combined with light-responsive modifications, photothermal hydrogels have gained much attention as effective steam generators producing fresh water using solar energy.<sup>[7]</sup>

In contrast, membranes are typically two-dimensional or thin-film structures with varying degrees of permeability, designed to selectively transport or filter molecules. This permeability is primarily governed by precisely controlled pore or channel sizes. Incorporating photothermal materials into membranes enables light-to-heat conversion, which can increase the driving force for mass flux and alter pore sizes, thereby modulating the membrane's permeability. Unlike hydrogels, which focus on bulk fluid retention and biological compatibility, membranes prioritize controlled permeability and are used in applications such as solar desalination,<sup>[8]</sup> water or air filtration,<sup>[82]</sup> and energy

harvesting.<sup>[125]</sup> Membranes generally do not require softness and flexibility but instead, they often require structural integrity under stress.

The distinctions between photothermal hydrogels and photothermal membranes can be summarized: Photothermal hydrogels are highly hydrated, soft, flexible, and biologically compatible, making them ideal for applications in biological systems. By contrast, photothermal membranes are selectively permeable, structurally robust under stress, and primarily focused on controlling permeability.

#### 2.2.4. Stability of Photothermal Hydrogels and Photothermal Membranes

Stability is a major concern when employing photothermal hydrogels and photothermal membranes in a variety of applications. This includes both the structural and performance stability of the entire system under different stresses (mechanical, thermal, chemical) over extended periods. In practice, photothermal hydrogels or membranes may be exposed to various physical and chemical stimuli, such as repeated heating and cooling cycles, feed loading and unloading, and chemical reactions. Consequently, they may undergo extreme deformation and material degradation, adversely affecting their structural and performance stability.

Essentially, there are two key strategies to enhance the stability of photothermal hydrogel or membrane systems: 1) strengthening the component materials and 2) improving the bonding between them. Strengthening the component materials involves selecting and engineering the photothermal materials and matrix materials to be robust and resistant to various stresses. For example, organic photothermal agents such as dyes may degrade and even lose their photothermal efficiency as the dye molecules break down with light exposure. To avoid this structural and performance degradation, these organic photothermal agents should be replaced by other chemically stable photothermal materials such as metal oxides, metal nanoparticles, or carbon-based materials when designing a photothermal system for long-term usage. Likewise, methods that can make matrix materials more robust are effective in enhancing the structural stability of the entire system. Adjusting the cross-linking density of the hydrogel, utilizing double-network hydrogels, or incorporating reinforcing agents such as nanofibers have been proven to effectively enhance the structural stability of hydrogels.<sup>[126,127]</sup> Similarly, methods to improve the robustness of membranes include selecting high-strength materials, engineering surfaces, increasing the cross-linking density, and incorporating nanofibers or nanoparticles as reinforcing agents.<sup>[128–130]</sup>

Another key strategy for enhancing stability is to improve the bonding between photothermal materials and their host matrices, including physical hydrogen bonding, Van der Waals forces, and chemical covalent bonding. Selecting materials and optimizing the surface roughness and compatibility can boost the physical interaction between photothermal materials and their matrix. Chemical functionalization or plasma treatment can help form strong chemical bonds and adhesion. Incorporating cross-link agents or in situ (or one-step) synthesis for photothermal

hydrogels or membranes can produce systems with covalently bonded photothermal materials. In the case of interpenetrating networks, the photothermal materials and the host matrix can form a molecular-level intertwined structure. Adding interfacial agents can enhance the interface adhesion and, consequently, the bonding. Physical constraints can be implemented to mitigate the risk of material leaching and detachment.

### 3. Materials Design and Engineering

The fabrication of photothermal hydrogels and photothermal membranes involves incorporating photothermal materials into the base matrix. Consequently, two primary considerations arise when designing these materials: the choice of photothermal materials and the method of incorporating them into the matrix. The following sections will discuss the development of photothermal materials and their incorporation into hydrogels and membranes.

#### 3.1. Photothermal Materials

Photothermal materials, capable of capturing and converting light into heat, underpin the synthesis of photothermal hydrogels and membranes. Till now, a wide range of materials are found to exhibit the photothermal effect, including metal nanoparticles,<sup>[131]</sup> metal oxides/sulfides,<sup>[132–134]</sup> carbon-based nanomaterials,<sup>[135,136]</sup> MXenes,<sup>[137]</sup> polymers,<sup>[138,139]</sup> and organic dyes.<sup>[140]</sup>

Noble metal nanoparticles such as Au,<sup>[141–143]</sup> Ag,<sup>[144–147]</sup> and Pt<sup>[148]</sup> exhibit strong absorption in the near infrared region for the light-to-heat conversion due to the localized surface plasmon resonance (LSPR) (Figure 2a(i)). Depending on the size, shape, and materials of the metal nanoparticles, LSPR occurs at specific wavelengths where, in response to the incident light, the nanoparticles' conduction electrons oscillate collectively, generating heat through nonradiative decay or electromagnetic heating.<sup>[20,149,150]</sup> Furthermore, the photothermal conversion efficiency can be tuned by geometrical modifications such as designing asymmetric structures with sharp and tapered features where plasmonic heating effect is increased due to the enhanced electromagnetic fields.<sup>[151,152]</sup> On the other hand, structures with low-symmetry tends to exhibit broadband absorption with multiple plasmon peaks.

Metal oxides, such as TiO<sub>2</sub>, ZnO, BiOCl, Bi<sub>2</sub>O<sub>3</sub>, and metal sulfides like CuS and MoS<sub>2</sub><sup>[153–157]</sup> are commonly used as photothermal materials. Their photothermal effect arises from the generation of photoexcited electron–hole pairs followed by non-radiative relaxation via recombination, where they release energy as phonons instead of photons to the material lattice, leading to an increase in lattice and surrounding medium temperature (Figure 2a(ii)). The light absorption and nonradiative relaxation of metal oxides/sulfide relies on their electronic states, which can be controlled through doping or the introduction of defects. The photothermal conversion of semiconductor materials can also be improved by constructing hierarchical structures which enhances photon absorption through increased light scattering.<sup>[158,159]</sup>

Carbon-based nanomaterials, such as graphene, graphene oxides (GOs), reduced graphene oxides (rGO), carbon nanotubes (CNTs), and carbon black, exhibit strong absorption over a broad range of wavelengths from visible to NIR, owing to the electronic transition within their  $\pi$ -electron systems.<sup>[135,160–162]</sup> As shown in Figure 2a(iii),  $\pi$ -electrons can be excited from the ground state (highest occupied molecular orbital, HOMO) to a higher energy state (lowest unoccupied molecular orbital, LUMO) by absorbed photons to form excitons. With the nonradiative relaxation of these excitons, the absorbed energy is released as heat energy. To tune their photothermal properties, functional groups on the carbon-based materials can be modified. Another approach is to create porous carbon-based nanostructures with enhanced light absorption. The porous structure has a smaller effective refractive index, resulting in reduced reflection of light. The pores also act as microcavities to promote light confinement through multiple light scattering and reflection, significantly enhancing the material–light interaction.<sup>[163]</sup> Compared with noble metal nanoparticles and metal oxides/sulfides, carbon-based materials are superior in terms of chemical stability, light weight, and low cost.

MXenes are a class of 2D layer-structured transition metal carbides, nitrides, or carbonitrides with a general formula of  $M_{n+1}X_nT_x$ , where  $(n + 1)$  layers of transition metals (M) are interleaved with  $n$  layers of carbon or nitrogen (X), and  $T_x$  represents the surface terminations such as O, OH, F, and/or Cl.<sup>[164]</sup> Depending on the composition and surface termination, MXenes can exhibit either metallic or semiconducting characteristics. This results in light absorption either through surface plasmon resonance (SPR) in metallic MXenes or photo-induced excitons generation in semiconducting MXenes.<sup>[137]</sup> The absorbed light energy is then converted into heat through a nonradiative relaxation process. One key advantage of MXenes is that due to their multi-elemental composition, they possess a high level of versatility, designability and tunability to achieve the desired photothermal performance. The bandgap can be readily tuned by adjusting the number of layers, endowing them with a wide absorption band. Furthermore, these 2D nanomaterials are usually ultrathin, resulting in high photothermal conversion efficiencies as they respond rapidly to light and also possess high in-plane electron mobilities. Additionally, MXenes feature high thermal conductivity, which facilitates heat dissipation and make them suitable for photothermal applications.

Polyrrrole (PPy),<sup>[165,166]</sup> polyaniline (PANI),<sup>[167]</sup> polythiophene (PT),<sup>[168]</sup> polydopamine (PDA)<sup>[169]</sup> are typical conjugated polymers that display photothermal effect. Upon exposure to light, these conjugated polymers absorb photons to induce electronic transition of the delocalized  $\pi$ -electrons from the ground state to an excited state.<sup>[138]</sup> The excited electrons then return to the ground state, releasing thermal energy via a nonradiative decay. The molecular structures of conjugated polymers are often tailorable, allowing for easy adjustment of their electronic structure to tune their light absorption and hence photothermal properties. Organic dyes, such as indocyanine green (ICG), and cyanine dyes, are widely used in biomedical imaging and photothermal therapy due to their strong light absorption in the NIR region and efficient light-to-heat conversion through nonradiative decay.<sup>[140,170]</sup>

## 3.2. Engineering Photothermal Materials into Photothermal Hydrogels and Membrane

After a brief introduction of the photothermal materials, the methods of integrating these materials into hydrogels and membranes will be discussed. Generally, these incorporation methods can be divided into two groups: one-step and two-step approaches.

### 3.2.1. One-Step Approach

The one-step approach refers to a simple and straightforward way of preparing photothermal hydrogels or membranes in a single process. This involves using photothermal materials either as precursors or by introducing them into the precursors for hydrogel or membrane fabrication. Within the hydrogel or membrane, photothermal materials are often well-blended with the matrix to achieve a uniform photothermal effect. 2D photothermal nanosheets, including GO, rGO, and MXenes are frequently used as building blocks for fabricating photothermal membranes through nanosheet assembly. For example, rGO flakes as the photothermal component were added to a suspension of *gluconacetobacter hansenii*, the precursor solution for synthesizing bacterial nanocellulose (BNC) fibers (Figure 3a). After an in situ BNC growth process, rGO flakes were successfully integrated with BNC fibers, forming a rGO/BNC photothermal membrane. When exposed to light ( $2.9 \text{ kW m}^{-2}$ ) for just 10 s, a rapid temperature increase from 25 to 60 °C was observed on this rGO/BNC photothermal membrane, while a counterpart without rGO showed only a subtle temperature increase of 3 °C, even with an extended exposure time of 120 s.<sup>[171]</sup> Additionally, 2D photothermal nanosheets can be used as primary building blocks for preparing photothermal membranes. By a vacuum-assisted filtration process, 2D  $Ti_3C_2T_x$  nanosheets were assembled into a membrane that exhibited a temperature rise from 23 to 42 °C under light illumination ( $1 \text{ W cm}^{-2}$ ) for 15 min.<sup>[172]</sup> In these 2D nanosheets stacked membranes, other photothermal materials, such as carbon quantum dots, metal nanoparticles, and CNTs,<sup>[173,174]</sup> can be incorporated to further enhance the photothermal effect. For instance, by facilitating in situ growth of Au NPs within the aforementioned  $Ti_3C_2T_x$  MXene membrane, the temperature can further increase to 47 °C under the same illumination conditions.<sup>[172]</sup>

In addition to directly using photothermal materials for fabricating hydrogels or membranes, these materials can be introduced into the precursors during the synthesis of hydrogels or membranes. For example, Ho's group imparted photothermal effect to a PNIPAM hydrogel by adding Au NPs to the precursor solution during hydrogel cross-linking.<sup>[143]</sup> The introduction of Au NPs significantly suppressed the light reflectance compared to hydrogels without Au NPs, indicating enhanced light absorption. Consequently, under solar irradiation, the temperature of the Au-incorporated hydrogel quickly rose from room temperature to 53 °C within 5 min, demonstrating its excellent light-to-heat conversion capability. Similarly, a  $Cs_xWO_3$ -infused PAM photothermal hydrogel was prepared by crosslinking acrylamide (AM, monomer) and cross-linkers in the presence of

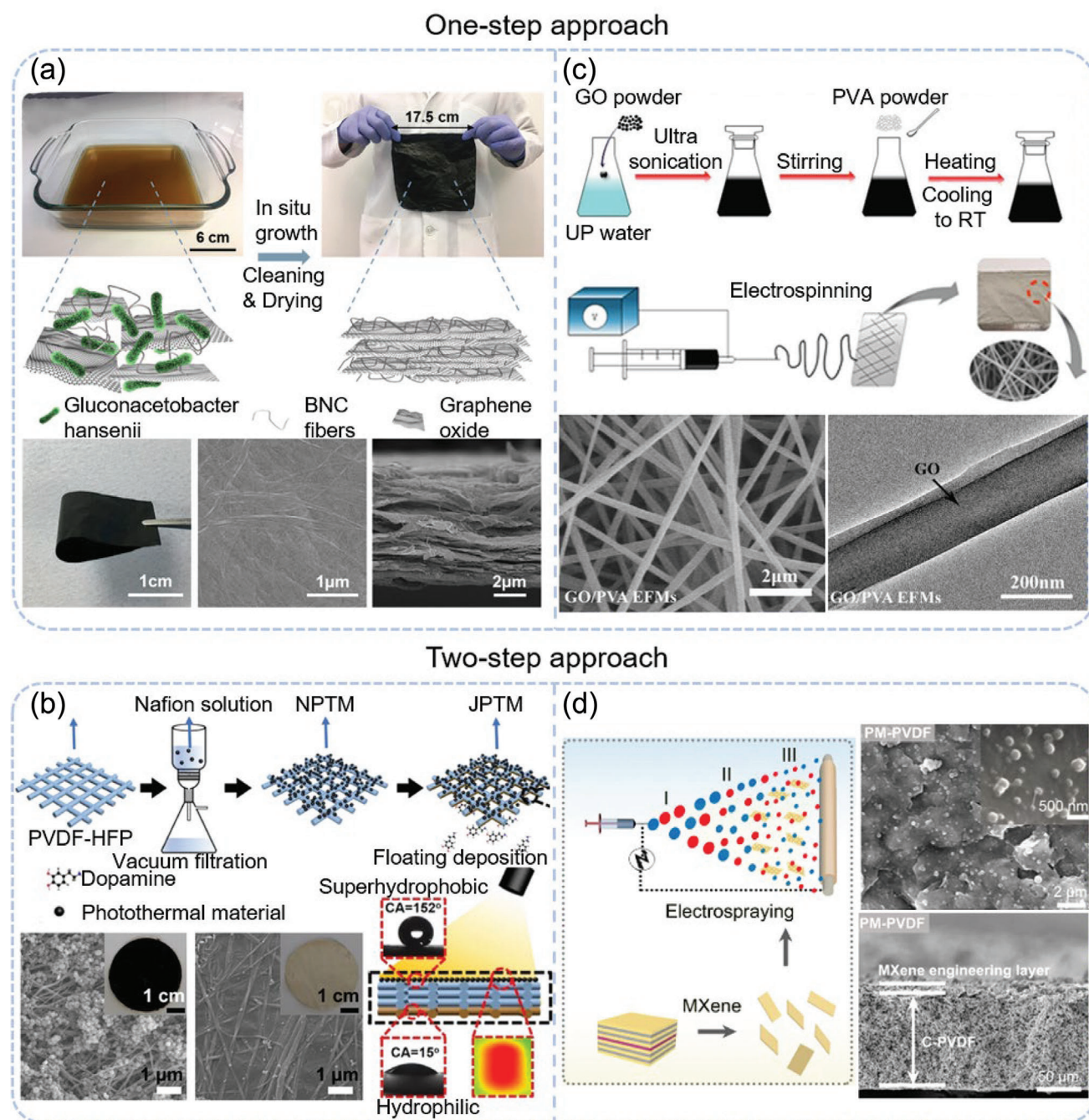


**Figure 3.** Fabrication of rGO/BNC membrane with the corresponding SEM images of the surface and cross-section. Reproduced with permission.<sup>[171]</sup> Copyright 2019, American Chemical Society. b) Schematic diagram of the preparation of the JPTM, Reproduced with permission.<sup>[176]</sup> Copyright 2021, American Chemical Society. c) Schematic diagram for the preparation of the GO/PVA EFMs and the corresponding SEM and TEM images. Reproduced under terms of the CC-BY license.<sup>[178]</sup> Copyright 2020, Elsevier. d) Schematic illustration of electrospinning process of MXene onto PVDF membrane and the corresponding SEM images of the surface and cross-section. Reproduced with permission.<sup>[179]</sup> Copyright 2022, Springer Nature.

$Cs_xWO_3$  nanorods.<sup>[175]</sup>  $Cs_xWO_3$  nanorods are photothermal materials with excellent absorption in the NIR region and high transmittance in the visible light region. As a result, the  $Cs_xWO_3$ -PAM hydrogel can be heated by light illumination while maintaining more than 70% transparency, making it promising for applications in wound visualization and accelerated healing.

### 3.2.2. Two-Step Approach

In the two-step approach, the introduction of photothermal materials occurs after the preparation of the matrix. In other words, the photothermal materials are incorporated into a prepared hydrogel or membrane. This facilitates modifications of many

commercial matrices, yielding products with wide applicability. Additionally, this two-step approach allows the construction of asymmetric structures, potentially introducing features that would otherwise be absent in symmetric structure. Poly(vinylidene fluoride) (PVDF) and its derivatives are often used for membrane distillation (MD), a membrane-based evaporation technology for desalination and separation. MD is known to suffer from intrinsic temperature polarization, resulting in performance degradation.<sup>[22]</sup> To address this, photothermal materials such as PDA, MXene, PPy, graphitic carbon spheres, are coated onto PVDF and PVDF-derived membranes, producing photothermal membranes. As shown in Figure 3b, graphitic carbon spheres (GCSs) were coated on a poly(vinylidene fluoride)-co-hexafluoropropylene (PVDF-HPF) membrane to grant this membrane photothermal function. Besides the photothermal effect, the GCSs coating also works as the hydrophobic top layer, which, together with the hydrophilic PDA bottom layer, produces a membrane with an asymmetric Janus structure. Owing to the photothermal layer and the asymmetric structure, high photothermal efficiency and accelerated mass transport were demonstrated in this Janus photothermal membrane, yielding a distillation flux of  $1.29 \text{ kg m}^{-2} \text{ h}^{-1}$ , 10 times higher than that of the conventional unmodified PVDF-HFP membrane.<sup>[176]</sup> The two-step approach can fabricate or modify membranes with asymmetries in terms of heating, wettability, porous structure, creating conditions favorable for MD, such as a greater temperature gradient and accelerated gas and liquid transport.

Both the one-step and two-step approaches have their respective advantages and disadvantages. The one-step approach streamlines the production process by combining the formation of hydrogels or membranes with the incorporation of photothermal incorporation into a single step. This often results in a uniform distribution and stronger integration of photothermal materials within the structure, promoting even heat generation and reducing the risk of material leaching or detachment. However, the one-step approach has significant limitations, particularly with regard to material selection. Not all photothermal materials are compatible with precursors or can be directly assembled into hydrogels or membranes. Additionally, when photothermal materials are included in precursors, their interactions with the matrix may not be well-controlled, making it difficult to optimize the overall performance of the system.

For the two-step approach, photothermal materials are typically incorporated by coating or modifying the surface of a pre-existing matrix, such as a membrane. This method is particularly advantageous because there are numerous commercially available membranes with well-controlled pore and surface properties, as well as a variety of surface engineering methods. Consequently, the two-step approach provides greater flexibility in synthesizing photothermal membranes as well as tuning their properties. However, since the photothermal materials are added post-fabrication, the bonds formed in the two-step-fabricated photothermal membranes might not be as strong as those in the one-step approach. This presents a risk of material leaking and detachment. Under light irradiation, this detachment risk may be exacerbated due to uneven heat distribution across the system.

Generally, the one-step approach is often employed to prepare photothermal hydrogels because it ensures strong bonds and structural stability, which are preferred for a hydrogel net-

work that is comparatively less dense than membranes. For preparation of photothermal membranes, the choice between the one-step or two-step approaches depends on specific application requirements, such as the molecule characteristics (e.g., size, surface charge, chemical affinity, etc.) of the feeding liquid or gas. Notably, many scalable fabrication methods such as 3D printing,<sup>[177]</sup> electrospinning (Figure 3c),<sup>[178]</sup> spraying (Figure 3d),<sup>[179]</sup> surface patterning,<sup>[180]</sup> and mode casting<sup>[181]</sup> are also applicable for the fabrication of photothermal hydrogels and membranes, whether adopting the one-step or two-step approaches.

## 4. Versatile Functionalities Across Multiple Fields

Photothermal hydrogels and membranes exhibit high levels of versatility because the structure of the matrix and the composition of active materials in the matrix can be easily customized and tailored to meet the demands of the desired applications. As a result, they are used in many different applications across multiple fields contributing to sustainability. In this section, the discussion will be focused on 3 sectors, namely 1) chemical fuel and clean water production, 2) electricity generation, and 3) mechanical actuator and robotics.

### 4.1. Chemical Fuel and Clean Water Production

Hydrogels and membranes serve as ideal platforms for generation of fuels such as hydrogen gas and hydrocarbons, as well as for the production of clean water (Table 1). This stems from their unique ability to embed the photothermal catalysts within the hydrogel and membrane matrix<sup>[182]</sup> or to facilitate in situ synthesis of catalytic materials during the hydrogel and membrane formation process.<sup>[183]</sup> In many of these fuel production applications, hydrogels act as hosts for catalysts, allowing for a 3D architecture of active materials which creates a conducive microscopic environment for the catalysts-reactant interactions, greatly enhancing catalytic performance.<sup>[184]</sup> The 3D structure not only provides an anchoring framework for the catalysts, but also provides an efficient electron transport pathway for enhanced catalytic activity. In some cases, hydrogels are designed as self-sustaining all-in-one reactors, eliminating the need for an external macro environment.<sup>[185]</sup> This streamlined design enhances efficiency and simplifies the fuel generation process.

#### 4.1.1. Fuel Production

Hydrogen is a high-energy-density fuel that burns cleanly, producing only water as its end product.<sup>[186]</sup> In typical photocatalyst systems, powdered catalysts are usually suspended in water which requires stirring. Alternatively, the catalysts can be immobilized in a bed reactor system. However, both systems present drawbacks such as stirring requirements, reduced reactant contact and difficulty in recovering and recycling photocatalysts. These issues can be resolved by using the photocatalyst in the form of a hydrogel or a membrane. Hydrogels are primarily utilized in hydrogen fuel production mainly as catalyst carriers

**Table 1.** Summary of performance metrics for chemical fuel and clean water production (light source is 1 kW m<sup>-2</sup> Xenon lamp (1 sun) unless stated otherwise).

Application	Photothermal material	Hydrogel/membrane material	Synthesis of composite	Production rate	Advantages	Refs.
H <sub>2</sub> production	CdSe/CdS nanorods	Nanocrystal-based hydrogel	Direct gelation	H <sub>2</sub> : 300 μmol g <sup>-1</sup> h <sup>-1</sup> (461% enhancement)	Overcomes issue of colloidal instability	[188]
	Au/g-C <sub>3</sub> N <sub>4</sub> nanoparticles	PNIPAM hydrogel	Mixed into gel precursor then gelation	H <sub>2</sub> : 1061.82 μmol g <sup>-1</sup> h <sup>-1</sup> (550% enhancement)	Adaptively direct its light-receiving area towards the light source	[190]
	Pt/C <sub>3</sub> N <sub>4</sub> nanosheets	PNIPAM and alginate hydrogel	Mixed into gel precursor then gelation	H <sub>2</sub> : 7437 μmol g <sup>-1</sup> h <sup>-1</sup> (130% enhancement)	Hydrogels act as a water reservoir	[185]
	Pt/TiO <sub>2</sub> nanoparticles	Polyurethane-poly(propylene glycol) hydrogel	Mixed into gel precursor then gelation	H <sub>2</sub> : 163 mmol h <sup>-1</sup> m <sup>-2</sup> (1.2 sun)	Floatable photocatalytic platform and photoreform plastic waste	[191]
CO <sub>2</sub> reduction	ZIF-67	Electrospun PAN nanofiber membranes	In situ growth	CO: 39.25 mmol g <sup>-1</sup> h <sup>-1</sup> (400 nm UV-cutoff filter)	Uniform distribution of photocatalytic active centers	[192]
	Co nanoparticles	Anodic aluminum oxide (AAO) membrane	Sputtering	CO: 1352 mmol g <sup>-1</sup> h <sup>-1</sup> (25 suns)	Nanoarray structure exhibits better light absorption, large channel size of the AAO facilitates gas diffusion	[193]
Clean water	Carbonized Fe-MOF nanoparticles	Konjac glucomannan (KGM) and PVA hydrogel network	Mixed into gel precursor then gelation	Evaporation: 3.2 kg m <sup>-2</sup> h <sup>-1</sup>	Removal of heavy metal ions and organic dyes	[200]
	rGO and Ti <sub>3</sub> C <sub>2</sub> T <sub>x</sub> MXene nanosheets	PVA and chitosan (CS) hydrogel	Mixed into gel precursor then gelation	Evaporation: 3.62 kg m <sup>-2</sup> h <sup>-1</sup>	Pyramid-shaped surface topography enhances water evaporation rate	[180]
	Polypyrrole (PPy)	Cationic hydrogel ([2-(methacryloyloxy)ethyl] trimethylammonium chloride (METAC))	Mixed into gel precursor then gelation	Evaporation: 1.59 kg m <sup>-2</sup> h <sup>-1</sup>	Nearly 100% antibacterial performance against <i>Escherichia coli</i> ( <i>E. coli</i> ) and <i>Staphylococcus aureus</i> ( <i>S. aureus</i> )	[203]
	Carbonized carboxymethyl chitosan (C-CMCS)	Alginate hydrogel	Mixed into gel precursor then gelation	Evaporation: 2.24 kg m <sup>-2</sup> h <sup>-1</sup>	Absorbs and photodegrades VOCs (95.37% removal rate of phenol)	[206]
	Ti <sub>3</sub> C <sub>2</sub> MXene and CdS nanoparticles	PAM hydrogel	Impregnation into hydrogel	Evaporation: 1.80 kg m <sup>-2</sup> h <sup>-1</sup>	Synergistic effects of photothermal evaporation and photocatalysis	[202]
Fuel and clean water	RhCrO <sub>x</sub> -Al: SrTiO <sub>3</sub>	Carbon paper membrane	Drop casting	H <sub>2</sub> : 16.1 mmol m <sup>-2</sup> h <sup>-1</sup> Evaporation: 0.94 kg m <sup>-2</sup> h <sup>-1</sup>	Use on a range of open-water sources (e.g., river, sea, water reservoir or industrial waste)	[207]
	Ag/TiO <sub>2</sub> nanofibers	Chitosan hydrogel	Mixed into gel precursor then gelation	H <sub>2</sub> : 5190 μmol m <sup>-2</sup> Evaporation: 5 kg m <sup>-2</sup> (5 hours illumination)	Vertically aligned pores afford high solar absorption, effective heat confinement, and rapid mass transport	[23]
	ZnIn <sub>2</sub> S <sub>4</sub> nanoclusters and PPy nanoparticles	PAN nanofiber film membrane	Electro-spinning and in situ growth	CO: 21.29 μmol g <sup>-1</sup> h <sup>-1</sup> Evaporation: 1.45 kg m <sup>-2</sup> h <sup>-1</sup>	All-in-one membrane with high porosity and an interconnected fibrous structure promotes localized photothermic vaporization	[209]

or electrolyte matrices in water splitting processes. Their high-water content and porous structure facilitate efficient transport of reactants and products. Additionally, their structured environment improves the stability and dispersion of catalysts, leading to more controlled and efficient reactions. Hydrogels also aid in the recovery and recycling of catalysts by immobilizing catalysts within their networks. Moreover, this immobilization prevents aggregation or precipitation of the catalysts, eliminating the need for continuous stirring. The use of hydrogel can pave the way

to a cleaner and more sustainable way of producing hydrogen by minimizing catalyst waste and the energy input required for stirring.<sup>[187]</sup>

Schlenkrich et al. demonstrated that a nanocrystal-based hydrogel, containing CdSe quantum dots, CdS nanorods, or CdSe/CdS dot-in-rod-shaped nanorods, exhibits a higher rate of hydrogen production rate than its ligand-stabilized nanocrystal solution counterpart.<sup>[188]</sup> This network of nanocrystals overcomes the issue of colloidal instability in photocatalysis, and

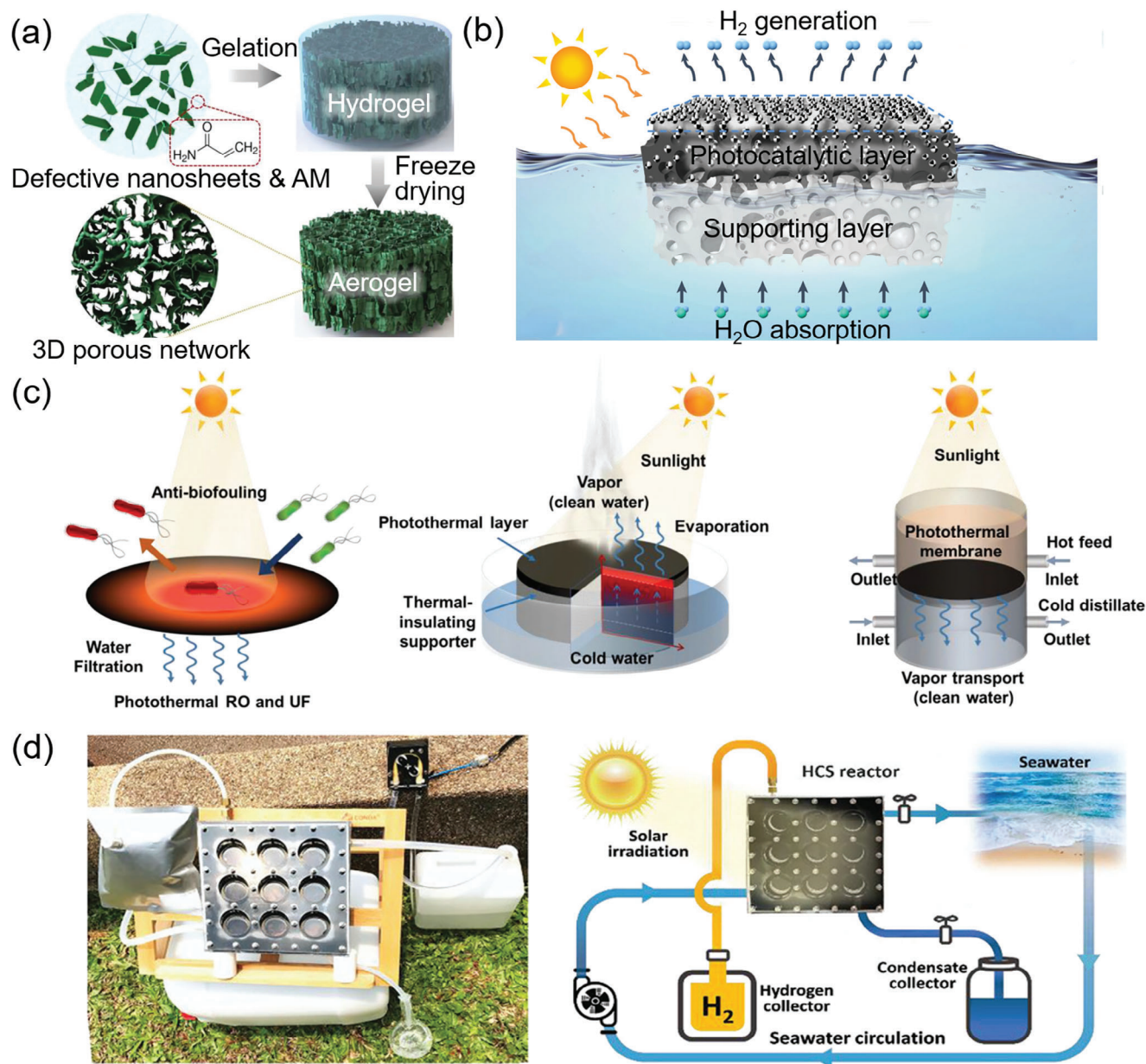


**Figure 4.** a) Schematic illustration for the synthesis of the defective D-HNb<sub>3</sub>O<sub>8</sub>/PAM aerogel. Reproduced with permission.<sup>[189]</sup> Copyright 2020, Wiley-VCH. b) Schematic of the floatable photocatalytic platform made up of porous elastomer–hydrogel nanocomposites for photocatalytic hydrogen generation. Reproduced with permission.<sup>[191]</sup> Copyright 2023, Springer Nature. c) Schematics showing the utilization of photothermal membranes in different water treatment systems. Reproduced with permission.<sup>[197]</sup> Copyright 2019, American Chemical Society. d) Digital photo and schematic diagram of the set-up for outdoor testing of the integral PTC gel prototype for concurrent photocatalysis and desalination of seawater under natural sunlight. Reproduced with permission.<sup>[23]</sup> Copyright 2020, Wiley-VCH.

facilitates photocatalytic hydrogen production without a co-catalyst. Furthermore, by maintaining the catalysts in a dispersed state, hydrogels and membranes aid in enhancing the accessibility of catalytic sites and improve the efficiency of reactions. Yang et al. produced a polyacrylamide (PAM) framework monolith containing oxygen vacancy (O<sub>v</sub>) defect-rich semiconductor HNb<sub>3</sub>O<sub>8</sub> (D-HNb<sub>3</sub>O<sub>8</sub>) nanosheets (Figure 4a) capable of full solar energy conversion.<sup>[189]</sup> The photothermal gel composite exhibited energy harnessing-conversion capability together with de-

sirable characteristics of capillary pumping, rapid mass diffusion and reactant enrichment, resulting in highly efficient photochemical activity. In some instances, hydrogels can be designed to respond to their environment to enhance the photocatalytic performance. Chen et al. developed a hydrogel from PNIPAM and gold-decorated carbon nitride (Au/g-C<sub>3</sub>N<sub>4</sub>) nanoparticles.<sup>[190]</sup> This photoactive hydrogel can adaptively direct its light-receiving area towards the light source to maximize its energy harvesting efficiency. This offers a new possibility for large scale deployment

of photocatalytic devices on water bodies or even sub-water surface where the device can track the sun's position for optimal hydrogen production.

Another advantage of hydrogels is their ability to act as a water reservoir, allowing them to function without an external water environment. Lei et al. combined Pt atoms loaded g-C<sub>3</sub>N<sub>4</sub> nanosheets with a 3D hydrogel network which enhances light absorption and charge carrier separation, yielding a hydrogen evolution performance 130% higher than that of the bare powder suspended in water.<sup>[185]</sup> Moreover, the water stored in the hydrogel can serve as a water reservoir for photocatalytic water splitting, demonstrating the possibility for the photocatalyst to operate efficiently without an external water environment. On the same note, Lee et al. demonstrated large scale hydrogen generation by designing a floatable photocatalytic platform made up of porous elastomer-hydrogel nanocomposites (Figure 4b).<sup>[191]</sup> The composite gel was able to generate hydrogen in seawater and photoreform plastic waste, and remained stable even after 14 days. A 1 m<sup>2</sup> prototype of the platform containing single-atom Cu/TiO<sub>2</sub> photocatalysts was able to produce 79.2 ml of hydrogen in a day under natural sunlight.

Besides hydrogen generation, photothermal membranes can be used in CO<sub>2</sub> reduction to mitigate the environmental issue related to greenhouse gas emissions. Moreover, they can facilitate the production of useful products such as CO, HCOOH, among others. Lin et al. deposited ZIF-67 on polyacrylonitrile (PAN) nanofiber membranes (NFMs) using an in situ growth technique for photocatalytic reduction of CO<sub>2</sub>.<sup>[192]</sup> Compared to ZIF-67 powder, the deposition of ZIF-67 nanocrystals on the nanofiber membrane produced a more uniform distribution of photocatalytic active centers, resulting in better CO<sub>2</sub> reduction performance. Moreover, the improved broad-spectrum light absorption of the composite membrane resulted in an enhanced photothermal effect which elevated the CO production rate to about 39,250 μmol g<sup>-1</sup> h<sup>-1</sup>. Lou et al. also created a membrane for photothermal CO<sub>2</sub> hydrogenation by sputtering Co nanoparticles onto an anodic aluminum oxide (AAO) membrane.<sup>[193]</sup> Compared to powder catalysts, such a nanoarray structure exhibits better light absorption and can be easily recycled. Moreover, the large channel size of the AAO facilitates gas diffusion and boosts the photothermal catalytic performance. As a result, a record Co-based photothermal CO production rate of 1352 mmol g<sub>Co</sub><sup>-1</sup> h<sup>-1</sup> was achieved.

#### 4.1.2. Clean Water

Clean water production is essential to the survival of all ecosystems, making it urgent to develop efficient, low cost, sustainable and scalable technologies to generate freshwater from bulk water, seawater or waste water.<sup>[194,195]</sup> Photothermal hydrogels and membranes have been demonstrated as a promising strategy for clean water production via sustainable solar energy.<sup>[196,197]</sup> The porous networks and tunable chemical composition of photothermal hydrogels provide a platform to incorporate photothermal absorbers, and the hydrophilic property of the cross-linked network further endows the photothermal hydrogel with superior water uptake capacities, ensuring an adequate water supply in the photothermal steam generation process.<sup>[180]</sup> Similarly, the introduction of solar energy in photothermal membranes can improve the

membrane efficiency during water purification.<sup>[21,198]</sup> Photothermal membranes have been widely used for four water purification applications (Figure 4c), namely reverse osmosis (RO), ultrafiltration (UF), solar steam generation (SSG) and membrane distillation (MD).<sup>[197]</sup> The localized photoheating of photothermal membranes deactivates microorganisms, improving the membrane's resistance to fouling during RO and UF, while SSG and MD membranes are able to treat highly saline water, industrial and municipal wastewater.<sup>[199]</sup>

The key components of photothermal hydrogels and membranes for clean water are the photothermal conversion materials and the hydrogel or membrane support. A promising photothermal conversion material should possess excellent absorption capacity for solar energy across the full wavelength range, good thermal insulation, and anti-corrosion properties in polluted water. Metals, semiconductors, carbon materials and polymer materials are generally good candidates for efficient photothermal conversion. For example, iron-based metal-organic framework (Fe-MOF)-derived photothermal nanoparticles,<sup>[200]</sup> MoS<sub>2</sub>,<sup>[201]</sup> rGO,<sup>[180]</sup> MXene,<sup>[202]</sup> and polypyrrole (PPy)<sup>[203]</sup> have been chosen as photothermal absorbers for various photothermal clean water production methods. Hydrogels and membranes serve as stable and versatile platforms that can accommodate photothermal absorbers, but more importantly, photothermal hydrogels have been reported to be able to lower the vaporization enthalpy due to the interaction between water molecules and polymer chains, thus achieving a more efficient water evaporation rate.<sup>[204]</sup> Guo et al. introduced konjac glucomannan (KGM) with Fe-MOF derived photothermal nanoparticles into PVA networks to form the photothermal hydrogel evaporator.<sup>[200]</sup> Due to the hydroxyl groups of KGM, the designed photothermal hydrogel has a high water evaporation rate and removal efficiency of heavy metal ions and organic dyes. Furthermore, different synthesis and post-modifications of photothermal hydrogels and membranes can be applied to enhance the solar-driven steam generation performance (Figure 4d).<sup>[205]</sup> Lu et al. designed a 2D nanostructure-embedded hybrid hydrogel by incorporating rGO and MXene nanosheets into PVA and chitosan (CS).<sup>[180]</sup> The surface topography of the photothermal hydrogel was designed with pyramid-shaped surface patterns, which aided in achieving a superior water evaporation rate of 3.62 kg m<sup>-2</sup> h<sup>-1</sup>. Besides solar evaporation, clean water can also be obtained through atmospheric water harvesting using photothermal hydrogels. Yilmaz et al. synthesized a thermo-responsive PNIPAM hydrogel consisting of MIL-101(Cr) loaded with Au nanoparticles. The hydrophilic PNIPAM with MIL-101(Cr) absorbs moisture from the air which is subsequently released as liquid water via the photothermal effect. When light is irradiated onto the photothermal Au nanoparticles, the light is converted into heat, raising the temperature of PNIPAM above the lower critical transition temperature (LCST ~ 32 °C), initiating a hydrophilic to hydrophobic phase transition in PNIPAM. This results in the expulsion of water from the PNIPAM matrix, demonstrating an autonomous water release and stand-alone airborne water supply system that has no moving parts.<sup>[143]</sup>

However, the accumulation of microorganisms from wastewater on photothermal hydrogels and membranes can lead to the deterioration of water transportation, resulting in produced freshwater of inferior quality and unsuitable for practical

applications. Peng et al. developed cationic photothermal hydrogels that not only produce freshwater but also inhibit bacteria growth.<sup>[203]</sup> These floating photothermal hydrogels can achieve a rapid water evaporation rate of  $1.592 \text{ kg m}^{-2} \text{ h}^{-1}$  and nearly 100% antibacterial performance against *Escherichia coli* (*E. coli*) and *Staphylococcus aureus* (*S. aureus*) (Figure 4e). Besides microorganisms, some organic contaminants in the wastewater such as volatile organic compounds (VOCs), might also be present in the collected freshwater. This is because the temperature at the water-gas interface of photothermal hydrogels and membranes is typically higher than  $60 \text{ }^\circ\text{C}$ , causing VOCs to evaporate together with water, leading to the existence of VOCs in the collected water.<sup>[206]</sup> Recently, freshwater production and simultaneous removal of VOCs during photothermal water evaporation have attracted much attention. An et al. developed a carbonized carboxymethyl chitosan (C-CMCS)/sodium alginate (SA) hydrogel solar evaporator (CSE) to realize simultaneous clean water production and removal of VOCs from wastewater.<sup>[206]</sup> The CSE not only serves as the photothermal absorber, it also absorbs and photodegrades VOCs to realize evaporation–absorption–degradation processes (Figure 4f). Wang et al. reported a MXene/CdS photothermal–photocatalytic hydrogel with a water evaporation rate of  $1.80 \text{ kg m}^{-2} \text{ h}^{-1}$  and a typical VOC (phenol) photodegradation rate of 85.12%.<sup>[202]</sup> These applications further broaden the scope of photothermal hydrogels and membranes for clean water generation from various water sources.

#### 4.1.3. Simultaneous Fuel and Clean Water Production

Although photocatalytic water splitting and  $\text{CO}_2$  reduction can directly convert solar energy into chemical energy in the form of hydrogen and hydrocarbon fuels, small amounts of contaminants in the water supply can severely deteriorate the performance and lifetime of the photocatalysis system. The water purification and transportation of clean water supply will further increase the operating cost of photocatalysis technology. Alternatively, coupling photocatalysis and water purification may address the issue of photocatalysts poisoning by contaminants in the water and also eliminate the condensation process,<sup>[207]</sup> necessary to produce clean water. More importantly, photothermal absorbers used for freshwater production can also promote photocatalytic activity by extending the light absorption range of the photocatalyst, boosting solar-to-chemical conversion efficiency.<sup>[17,208]</sup> Pornrungrroj et al. designed a hybrid system consisting of a photocatalyst  $\text{RhCrO}_x\text{-Al:SrTiO}_3$  and a solar vapor generator (SVG) for water purification and simultaneous water splitting to produce green hydrogen (Figure 4g).<sup>[207]</sup> Similarly, Gao et al. formulated a photothermal catalytic (PTC) gel from chitosan via an ice-templating method to create vertically aligned pores for parallel clean water and hydrogen production.<sup>[23]</sup> The gel containing Ag-decorated  $\text{TiO}_2$  nanofibers exhibited both interfacial solar heating for heat confinement and localized plasmonic heating at the catalyst active sites, leading to enhanced hydrogen production performance. An integral prototype for simultaneous hydrogen production and desalination of seawater under natural sunlight was also demonstrated (Figure 4h). Han et al. developed a compact double-stage solar-driven catalytic membrane distillation (DSCMD) system for simultaneous clean wa-

ter and  $\text{CO}_2$  conversion.<sup>[209]</sup> The photothermal catalytic nanofiber membrane is prepared by electrospinning of PAN polymer with  $\text{ZnIn}_2\text{S}_4$  photocatalyst and in situ growth of PPy nanoparticles as the solar absorber. This all-in-one membrane with high porosity and an interconnected fibrous structure promotes localized photothermic vaporization, and at the same time, the photothermal effect also acts on the catalytically active sites of adjacent  $\text{ZnIn}_2\text{S}_4$  to enhance  $\text{CO}_2$  photoreduction to produce CO.

In essence, photothermal hydrogels and membranes can produce clean water via solar evaporation and atmospheric water harvesting. Moreover, they serve as efficient catalyst carriers and electrolyte matrices in water-splitting and  $\text{CO}_2$  reduction processes, leveraging their high-water content and porous structure for improved reactant/product transport and catalyst stability. The inclusion of photothermal effect also enhances the efficiency of the catalytic reaction. Ideally, both the fuel and clean water production functions can be combined into a single system to achieve higher energy efficiency.

## 4.2. Electricity Generation

Integrating photothermal materials into hydrogels or membranes offers an effective approach for harnessing solar energy. The heat generated by these photothermal hydrogels or membranes can be converted into electricity through various mechanisms. These include combinations with thermoelectric, thermogalvanic, hydrovoltaic, salt gradient energy harvesting and others (Table 2 and Figure 5).

### 4.2.1. Thermoelectric

Thermoelectric (TE) technology operating on the “Seebeck effect” (the generation of a voltage across a material when subjected to a temperature gradient), offers a simple solution for direct heat-to-electricity conversion.<sup>[210,211]</sup> Light illumination can create a temperature gradient between the photothermal hydrogel or membrane (high temperature) and its surroundings (low temperature). By integrating TE technology, this temperature difference can be utilized to generate electricity (Figure 5a). Ho’s group reported a solar-driven steam-and-electricity co-generator consisting of a 3D polydimethylsiloxane (PDMS) gel coated with carbon nanotube/cellulose nanocrystal (CNT/CNC) (or PCC sponge) placed atop a TE module. As shown in Figure 5b, photothermal heating causes the PCC sponge to increase in temperature and the absorbed water to turn into steam. At the same time, the temperature at the top side of the TE module (near the PCC sponge) becomes higher than the bottom side (in the bulk water), and this temperature difference results in an electric output from the TE module.<sup>[212]</sup> Similar work of integrating TE for electricity generation can also be found in hydrogels of carbon nanotube/polyacrylamide (CNT/PAM)<sup>[56]</sup> and carbon black/ polyvinyl alcohol (CB/PVA),<sup>[213]</sup> and membranes of poly(*N*-phenylglycine) (PNPG)/ $\text{MoS}_2$ ,<sup>[214]</sup> carbon nanoparticles/polyvinyl alcohol (CN/PVA)-coated cotton fabric,<sup>[215]</sup> and graphene oxide–melanin (GOM) composite.<sup>[216]</sup>

**Table 2.** Summary of performance metrics for electricity generation (light source is 1 kW m<sup>-2</sup> Xenon lamp (1 sun) unless stated otherwise).

Application	Photothermal material	Hydrogel/membrane material	Synthesis of composite	$\Delta T$ (K)	Power output	Evaporation	Refs.
Thermoelectric with solar evaporation (commercial TE module)	CNT/cellulose nanocrystal (CNT/CNC)	PDMS hydrogel	Dip-coating	4.6	$V_{oc}$ : 60 mV, $I_{sc}$ : 26 mA Power density: 0.4 W m <sup>-2</sup>	1.36 kg m <sup>-2</sup> h <sup>-1</sup>	[212]
	CNT	PAM hydrogel	Mixed into gel precursor then gelation	55	$V_{oc}$ : 2.8 V, $I_{sc}$ : 65.8 mA Power density: 4.8 W m <sup>-2</sup> (Array of 8 home-made 4 cm x 4 cm TE modules)	1.42 kg m <sup>-2</sup> h <sup>-1</sup>	[56]
	Carbon black	PVA hydrogel	Mixed into gel precursor then gelation	15.9	$V_{oc}$ : 140 mV, $I_{sc}$ : 5.4 mA Power density: 0.63 W m <sup>-2</sup>	2.33 kg m <sup>-2</sup> h <sup>-1</sup>	[213]
	Poly(N-phenylglycine) (PNPG)/MoS <sub>2</sub>	Membrane	Electrostatic self-assembly and vacuum filtration	6	$V_{oc}$ : 110 mV, $I_{sc}$ : 12 mA Power density: 0.23 W m <sup>-2</sup>	1.70 kg m <sup>-2</sup> h <sup>-1</sup>	[214]
	Carbon nanoparticles/PVA (CN/PVA)	Cotton fabric membrane	Vacuum filtration	9	$V_{oc}$ : 160 mV, $J_{sc}$ : 33 A m <sup>-2</sup> Power density: 1.2 W m <sup>-2</sup> (4 suns)	4.51 kg m <sup>-2</sup> h <sup>-1</sup> (4 suns)	[215]
Thermo-galvanic	Graphene oxide (GO)	Melanin membrane	Drop casting	8	$V_{oc}$ : 50 mV, $I_{sc}$ : 14 mA Power density: 0.9 W m <sup>-2</sup>	1.35 kg m <sup>-2</sup> h <sup>-1</sup>	[216]
	PDMS-CuO/Cu foil film	PAM hydrogel (Cu <sup>0</sup> /Cu <sup>2+</sup> redox couple)	Layer by layer assembly	8.7	$V_{oc}$ : 10.3 mV, $J_{sc}$ : 0.8 A m <sup>-2</sup> Power density: 1.6 mW m <sup>-2</sup> Seebeck coefficient: 1.20 mV K <sup>-1</sup>	1.33 kg m <sup>-2</sup> h <sup>-1</sup>	[57]
	Pyrogallol acid (PA) and polyethyleneimine (PEI)	Polyacrylamide and carboxymethylcellulose (PAM-CMC) hydrogel (Fe(CN) <sub>6</sub> <sup>3-</sup> / Fe(CN) <sub>6</sub> <sup>4-</sup> redox couple)	Dip-coating	1.9	$V_{oc}$ : 6.92 mV, $J_{sc}$ : 0.75 A m <sup>-2</sup> Power density: 1.47 mW m <sup>-2</sup> Seebeck coefficient: -1.40 mV K <sup>-1</sup>	Nil	[218]
Hydrovoltaic	MWNTs, MXene, CsPbBr <sub>3</sub>	Cellulose hydrogel with ionic liquid of 1- <i>n</i> -butyl-3-methylimidazolium chloride (BMIMCl)	Mixed into gel precursor then gelation	Nil	$V_{oc}$ : 0.543 V, $I_{sc}$ : 121.4 $\mu$ A Power density: 11.8 $\mu$ W cm <sup>-2</sup> (2 suns)	2.78 kg m <sup>-2</sup> h <sup>-1</sup>	[219]
	Carbon nanoparticles	Al <sub>2</sub> O <sub>3</sub> plate membrane	Doctor blading	Nil	$V_{oc}$ : 1 V, $I_{sc}$ : 0.75 $\mu$ A Power density: 8.1 $\mu$ W cm <sup>-2</sup>	Nil	[220]
Osmotic or Reverse electrodialysis	Carbon black	Quartz membrane	Ethanol flame	Nil	$V_{oc}$ : 1 V, $I_{sc}$ : 0.15 $\mu$ A Power density: 53 nW	Nil	[221]
	Al <sub>2</sub> O <sub>3</sub> and carbon black particles	Polyethylene terephthalate (PET) membrane	Doctor blading	Nil	$V_{oc}$ : 5.86 V, $I_{sc}$ : 16.1 $\mu$ A m <sup>-1</sup> Power density: 24.4 $\mu$ W m <sup>-1</sup>	Nil	[222]
	CNT	Filter paper	Dip-coating	Nil	$V_{oc}$ : 60 mV, $I_{sc}$ : 3 mA cm <sup>-2</sup> Power density: 0.5 W m <sup>-2</sup> ( $\approx$ 10-fold NaCl gradient)	1.1 kg m <sup>-2</sup> h <sup>-1</sup>	[225]
	Black cotton	Graphene oxide membranes	Nil	Nil	Power density: 4.5 W m <sup>-2</sup> (50-fold NaCl gradient)	0.88 kg m <sup>-2</sup> h <sup>-1</sup>	[226]

(Continued)

**Table 2.** (Continued)

Application	Photothermal material	Hydrogel/membrane material	Synthesis of composite	$\Delta T$ (K)	Power output	Evaporation	Refs.
	Carbon (Chinese ink)	Cotton fabric	Dip-coating	Nil	$V_{oc}$ : 52 mV, $J_{sc}$ : 7.93 $\mu\text{A}$ Power density: 116.52 $\text{mW m}^{-2}$	1.94 $\text{kg m}^{-2} \text{h}^{-1}$	[227]
	Carbon black	Alginate hydrogel and Ni foam	Mixed into gel precursor then gelation	Nil	$V_{oc}$ : 0.9 V, $J_{sc}$ : 20.3 $\text{mA m}^{-2}$ Power density: 5.3 $\text{mW m}^{-2}$	2.1 $\text{kg m}^{-2} \text{h}^{-1}$	[228]
	Au NPs with polyoxometalates	Anodic aluminum oxide (AAO) membrane	Deposition	Nil	Power density: 70.4 $\text{W m}^{-2}$ (500-fold NaCl gradient) (532 nm laser, 2 $\text{kW m}^{-2}$ )	Nil	[229]
Others	Carbon sponge	Nil	Carbonization of melamine foam	Nil	$V_{oc}$ : -20 V, $J_{sc}$ : -80 nA Power density: 240.7 $\mu\text{W m}^{-2}$ (Pyro- and Piezoelectricity)	1.39 $\text{kg m}^{-2} \text{h}^{-1}$	[231]
	Au nanoflowers	Silica hydrogel	Mixed into gel precursor then gelation	Nil	$V_{oc}$ : $\approx 10$ V, $J_{sc}$ : 0.35 $\mu\text{A}$ Power: 0.63 $\mu\text{W}$ (Triboelectricity)	1.356 $\text{kg m}^{-2} \text{h}^{-1}$	[232]
	$\text{Al}_2\text{O}_3$ nanoparticles (hydrovoltaic)	Gelatin (thermoelectric) $(\text{Fe}(\text{CN})_6^{3-} / \text{Fe}(\text{CN})_6^{4-}$ redox couple)	Nil	4	$V_{oc}$ : 6.4 V, $J_{sc}$ : 700 nA (Hydrovoltaic)	Nil	[233]
	Carbon cloth	Nafion membrane (KI/KI <sub>3</sub> redox couple)	Nil	15	$V_{oc}$ : 4 mV, $J_{sc}$ : 30 $\mu\text{A cm}^{-2}$ (Thermoelectric)	1.4 $\text{kg m}^{-2} \text{h}^{-1}$	[234]
	Bismuth oxychloride (BiOCl)/carbon black (HBiC)	Alginate hydrogel	Mixed into gel precursor then gelation	Nil	$V_{oc}$ : 80 mV, $J_{sc}$ : 42.2 A $\text{m}^{-2}$ Power density: 0.65 $\text{W m}^{-2}$ (Thermogalvanic) $V_{oc}$ : 142 mV, $J_{sc}$ : 41.0 A $\text{m}^{-2}$ Power density: 1.45 $\text{W m}^{-2}$ (Reverse electrolysis)	2.51 $\text{kg m}^{-2} \text{h}^{-1}$	[235]

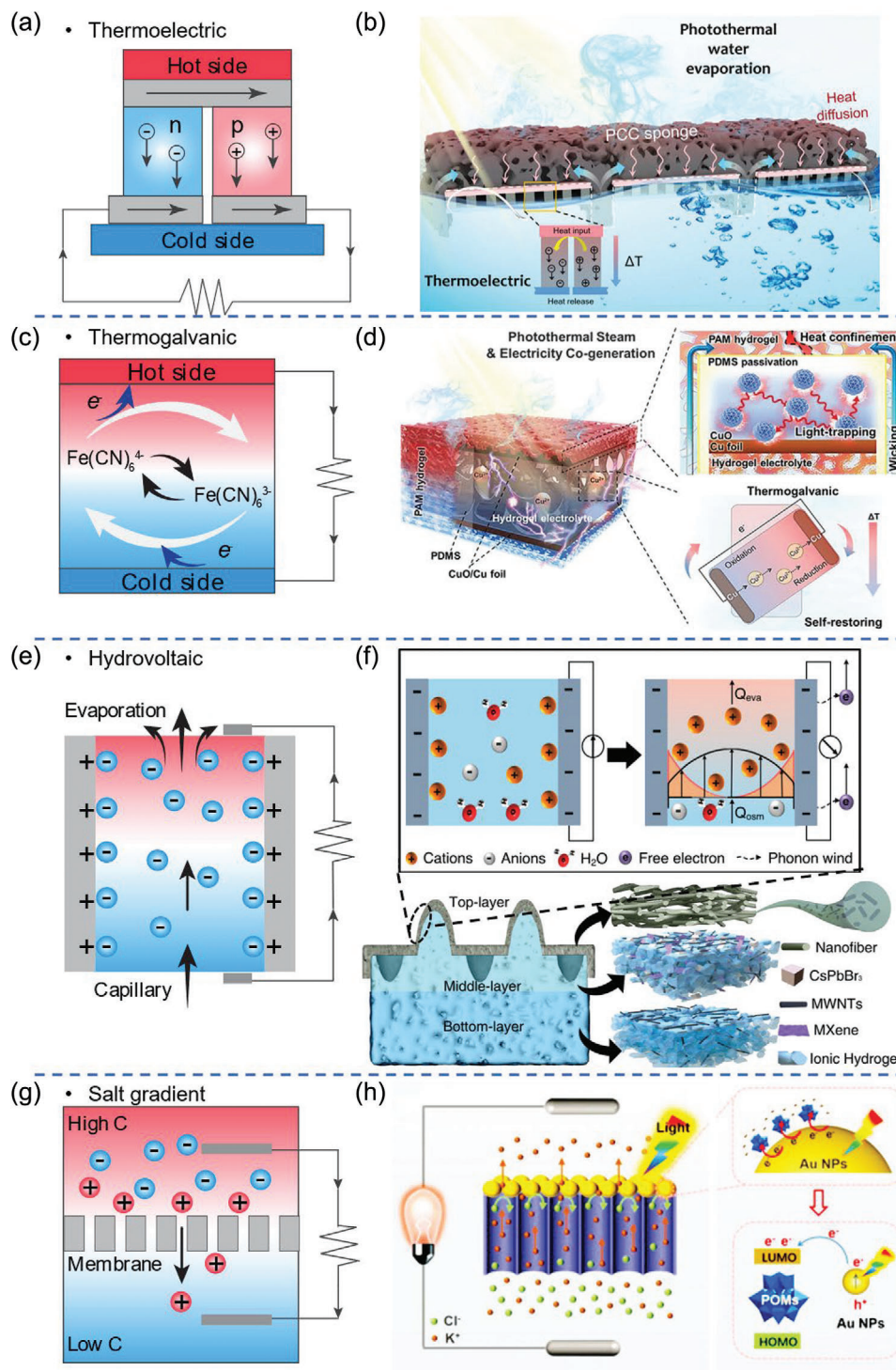


**Figure 5.** a) Schematic of a thermoelectric cell. b) Schematic of the PCC sponge on top of a TE module under solar irradiation. Reproduced with permission.<sup>[212]</sup> Copyright 2019, Wiley-VCH. c) Schematic of a thermogalvanic cell. d) Schematic of the integrated photothermal evaporator/thermogalvanic cell. Reproduced with permission.<sup>[57]</sup> Copyright 2020, Wiley-VCH. e) Schematic of a hydrovoltaic cell. f) Power generation principle for the IENG induced by water evaporation and the subsequent ion movement within the channel, and a schematic diagram of the composition of a fabricated IENG. Reproduced with permission.<sup>[219]</sup> Copyright 2022, Springer Nature. g) Schematic of a RED cell. h) Osmotic energy conversion using the prepared PESM. Reproduced with permission.<sup>[229]</sup> Copyright 2024, Springer Nature.

#### 4.2.2. Thermogalvanic

In addition to thermoelectric technology, thermogalvanic technology can also harness the temperature difference between the photothermal hydrogel/membrane and its surroundings to generate electricity. Thermogalvanic technology refers to the thermal voltage generation through temperature-dependent redox reactions at the cold and hot electrodes (Figure 5c).<sup>[217]</sup> Figure 5d illustrates a steam–electricity cogeneration system where a photothermal evaporator is integrated with a thermogalvanic cell. The photothermal evaporator consists of a PDMS-coated copper oxide/copper foil (PDMS-CuO/Cu foil) film as the light absorber and a PAM hydrogel as the water reservoir. The thermogalvanic cell includes an electrolyte-infused PAM hydrogel sandwiched between two CuO/Cu foil electrodes. When exposed to light, the PDMS-CuO/Cu foil absorbs light, inducing photothermal conversion for dual purposes. One is evaporating water in the upper PAM hydrogel to generate steam, and the other is establishing a temperature gradient across the thermogalvanic cell, which triggers the temperature-dependent redox reaction of copper/cupric sulfate at two electrodes, resulting in a voltage output from the thermogalvanic cell.<sup>[57]</sup> Another example is the coating of a mixture solution of pyrogallol acid (PA) and polyethyleneimine (PEI) as an interlocking photothermal layer on the surface of a polyacrylamide and carboxymethylcellulose (PAM-CMC) hydrogel infused with an  $\text{Fe}(\text{CN})_6^{3-}/\text{Fe}(\text{CN})_6^{4-}$  redox couple electrolyte. This converts the hydrogel into a solar-driven thermoelectrochemical cell, enabling the photo-thermo-electric conversion in this hydrogel to power sensors in a “smart home”.<sup>[218]</sup>

#### 4.2.3. Hydrovoltaic

Hydrovoltaic technology refers to electricity generation through the interaction between nanostructured materials with water in its diverse forms, including flowing liquids, moving droplets, fluctuating waves, as well as floating moisture.<sup>[118]</sup> Among them, flowing liquid and steam are commonly presented in applications of photothermal hydrogels or membranes, such as solar-driven evaporation. Additionally, most photothermal hydrogels or membranes have a micro-to-nanoscale porous structure, which significantly enhances the double electronic layer (EDL) at the liquid/material interface and thus facilitates selective ionic transport within these porous channels, ultimately translating into improved electricity generation. Therefore, combining hydrovoltaic technology with photothermal hydrogel or membrane can offer another effective method for achieving photo-thermo-electric conversion. As illustrated in Figure 5e, under light illumination, the evaporation (or transpiration force) and capillary force cause unidirectional water flow within the porous photothermal hydrogel or membrane, resulting in streaming potential along with steam generation.<sup>[116]</sup>

Figure 5f (bottom) shows a bioinspired multilayered interfacial evaporation-driven nanogenerator (IENG). The top layer is covered by nanofibers composed of multiwalled carbon nanotube (MWNTs). The middle layer is engineered with a mixture of hydrogel, MWNTs, MXene, and  $\text{CsPbBr}_3$ , structured like a moth-eye to maximize light absorption, while the bottom hydrogel layer

serves as the water supply. Under light irradiation, the moth-eye-structured middle layer significantly enhances light-to-heat conversion, increasing the water evaporation rate at the middle layer. The evaporation maintains the transpiration force and osmotic force that draw water rapidly from the bottom hydrogel to the top layer. When water contacts the MWNTs, electronic double layers are established at the water/MWNTs interface, facilitating cation transport. With solar-driven water escape from the top layer, a streaming potential is generated (top of Figure 5f).<sup>[219]</sup> Evaporation-induced electricity generation is also observed in membranes made from photothermal materials such as carbon nanoparticles.<sup>[220–222]</sup>

#### 4.2.4. Osmotic Energy Conversion

In addition to the temperature gradient, continuous evaporation can also create a salt gradient between the photothermal hydrogel or membrane and bulk water. This salt gradient can be utilized to generate electricity by osmotic energy conversion technology, or reverse electrodialysis (RED).<sup>[223,224]</sup> Figure 5g shows a RED cell consisting of two solution with different concentrations separated by a semipermeable membrane. With the selective ionic transport across the membrane, electrical output is generated between the two electrodes. Integrating osmotic energy conversion technology with photothermal hydrogels and membranes makes it possible to convert light energy into electricity. Covering a photothermal membrane on top of a RED cell,<sup>[225–227]</sup> or using a photothermal hydrogel as the RED cell,<sup>[228]</sup> generates electricity as solar-driven evaporation increases the salt concentration in the light-exposed cell. Moreover, the interaction of the photothermal membrane with light can be directly utilized to enhance electricity generation. For example, as illustrated in Figure 5h, when light is projected onto a polyoxometalates (POMs)-based nanofluidic plasmonic electron sponge membrane (PESM), hot electrons are generated on the surface of Au NPs and then transferred to and stored in POMs electron sponges. The stored hot electrons in POMs increase the charge density and hydrophilicity of PSM, significantly improving selectivity and thus the osmotic energy conversion performance.<sup>[229]</sup> Lao et al. demonstrated nanofluidic photothermal electricity generation through the use of  $\text{Ti}_3\text{C}_2\text{T}_x$  nanosheets. When the  $\text{Ti}_3\text{C}_2\text{T}_x$  nanosheets membrane is placed on an ionic solution and partially illuminated, the asymmetric light irradiation results in differential heating of the photothermal nanosheets, producing a water evaporation gradient. This in turn generates water flow from the slow evaporation region to the fast evaporation region through the nanofluidic channels in the membrane, which transports the cations and results in an ionic current.<sup>[230]</sup>

#### 4.2.5. Others

Apart from the four mechanisms discussed above, other strategies exist for achieving light-heat-electricity conversion. For example, Zhu et al. combined a PVDF film with a solar-driven evaporation gel system to harvest electricity from steam generation. Due to the pyroelectric property of PVDF, the steam-induced temperature fluctuations on the PVDF film are converted into

its oscillating electric output to harvest the thermomechanical responses from the carbon sponge (CS) solar-vaporization (Figure 6a).<sup>[231]</sup> In a system combining a triboelectric generator with a 3D plasmonic solar absorber gel, freshwater and electricity can be concurrently obtained when the solar-generated steam condenses and slides over the triboelectric generator (Figure 6b).<sup>[232]</sup>

Although these mechanisms have been discussed separately, they do not necessarily have to function individually. In fact, these mechanisms can work in combination to synergize solar-driven electricity generation mediated by photothermal hydrogels or membranes. Figure 6c shows such a multi-integrated system, where a flexible ionic thermoelectric gelatine gel was integrated with a porous Al<sub>2</sub>O<sub>3</sub>-based hydrovoltaic generator. When exposed to light, the thermoelectric gel produces electricity due to the solar-induced temperature gradient across it. Simultaneously, the thermoelectric cell enhances heat conduction between the hydrovoltaic generator and its environment, increasing the water evaporation rate and thereby boosting the output voltage of the hydrovoltaic generator. In turn, continuous water evaporation at the hydrovoltaic generator helps maintain a constant temperature difference for the thermoelectric generator. Synergistically, this multi-integrated system has achieved a stable voltage of up to 6.4 V.<sup>[233]</sup> Combining a thermogalvanic cell and reverse electro dialysis with solar-driven interfacial evaporation was also proposed to simultaneously extract energy from the temperature and salinity gradients created during evaporation, as illustrated in Figure 6d. This coupling can be engineered to enable mutual power enhancement, resulting in a steam-electricity cogeneration system that can yield evaporation rate of 1.4 kg m<sup>-2</sup> h<sup>-1</sup> and electricity output of 1.11 W m<sup>-2</sup> concurrently under one sun illumination.<sup>[234]</sup> Synergistic solar-driven desalination and photoelectrochemistry energy generation can also be achieved with a calcium alginate hydrogel embedded with bismuth oxychloride (BiOCl) and carbon black.<sup>[235]</sup> Under solar irradiation, BiOCl undergoes a photocorrosion process to produce Bi nanoparticles and chemical energy. The Bi nanoparticles generate photothermal heat to aid in the evaporation of water at a rate of 2.51 kg m<sup>-2</sup> h<sup>-1</sup>. At night, Bi is converted back to BiOCl by a unique autoxidation process where the stored chemical energy is converted into electrical energy by a Bi-air battery with a maximum current density of 15 μA cm<sup>-2</sup>.

In summary, photothermal hydrogels and membranes offer an effective approach towards harnessing solar energy and converting the photothermal heat into electricity. The availability of various routes such as thermoelectric, thermogalvanic, hydrovoltaic and salt gradient energy harvesting means that solar energy can be captured in various real-world scenarios, making it a highly effective technology.

### 4.3. Mechanical Actuator and Robotics

Light can also be used to drive mechanical actuation by infusing photothermal materials into hydrogels and membranes. The use of light as an energy source is advantageous because it is sustainable, and it allows for easy switching and precise manipulation. This is highly applicable for remote actuation and soft robotics, where light instead of electricity can be used to drive movement

in a remote, noncontact and controlled manner.<sup>[236,237]</sup> The principles of actuation can be broadly classified into asymmetric thermal expansion and light-induced Marangoni propulsion effect.

#### 4.3.1. Asymmetric Thermal Expansion

In asymmetric thermal expansion, the photothermal actuator experiences different degrees of expansion across the actuator when illuminated with light, causing it to be bent or distorted into different shapes, resulting in actuation motion. This asymmetry can be attributed to selective illumination on certain areas of the actuator, or it can also be achieved by combining materials with different coefficient of thermal expansion in the fabrication of the actuator.

A photothermal membrane actuator can be fabricated simply by coating polydopamine-modified reduced graphene oxide-carbon nanotube (PDG-CNT) onto 3D-aligned ferroelectric PVDF film as shown in Figure 7a.<sup>[238]</sup> Graphene has a negative coefficient of thermal expansion (CTE), while PVDF has a positive CTE. Hence, when exposed to light, the actuator will increase in temperature due to the photothermal effect, and the mismatch in CTE will cause the actuator to produce motion in various axes of movement such as translational oscillation, directional rolling, and rotation. The bimorph structure was cleverly designed with a self-generated cyclic shifting of center of gravity to create an in-built thermo-mechanical feedback system enabling perpetual locomotion. On top of mechanical actuation, the ferroelectric PVDF layer in the actuator can also produce electricity by harvesting the mechanical stress and temperature gradient simultaneously through piezoelectricity and pyroelectricity, respectively. Actuators like these demonstrate the potential for all-in-one thermo-mechano-electrical transduction, multigait soft energy robots and waste heat harvesting technologies. Employing a similar material composite concept, Wang et al. designed a light-driven thin-film actuator with self-powered somatosensory abilities, capable of detecting its body temperature and actuation deformation states (Figure 7b).<sup>[239]</sup> The active materials graphite-CNT composite and the ferroelectric PVDF enable perception of the deformation state and temperature utilizing piezoresistive and pyroelectric effects respectively. Furthermore, the composite material can be shaped and patterned into low-profile structures through the Japanese traditional art of kirigami for morphable, mobile, and multiple robotic functionalities. This soft robot with integrated perception and motility capabilities, offers new opportunities for developing diverse intelligent behaviors in soft robots.

Besides membranes, photothermal materials can also be integrated into hydrogels, especially thermo-responsive polymer materials such as PNIPAM which exhibits a reversible volume change due to a coil-to-globule transition above its LCST of ~32 °C.<sup>[240-242]</sup> Cheng et al. developed a PNIPAM-based photo-responsive ink for direct-ink-write (DIW) printing onto polydimethylsiloxane (PDMS) substrate (Figure 7c).<sup>[68]</sup> In this ink, multiwalled carbon nanotube (MWNT) serves as the photothermal component, and the silane coupling agent ensures strong interfacial bonding between the printed PNIPAM hydrogel and PDMS substrate. When the actuator is heated beyond its LCST via the light-induced photothermal effect of MWNTs, the

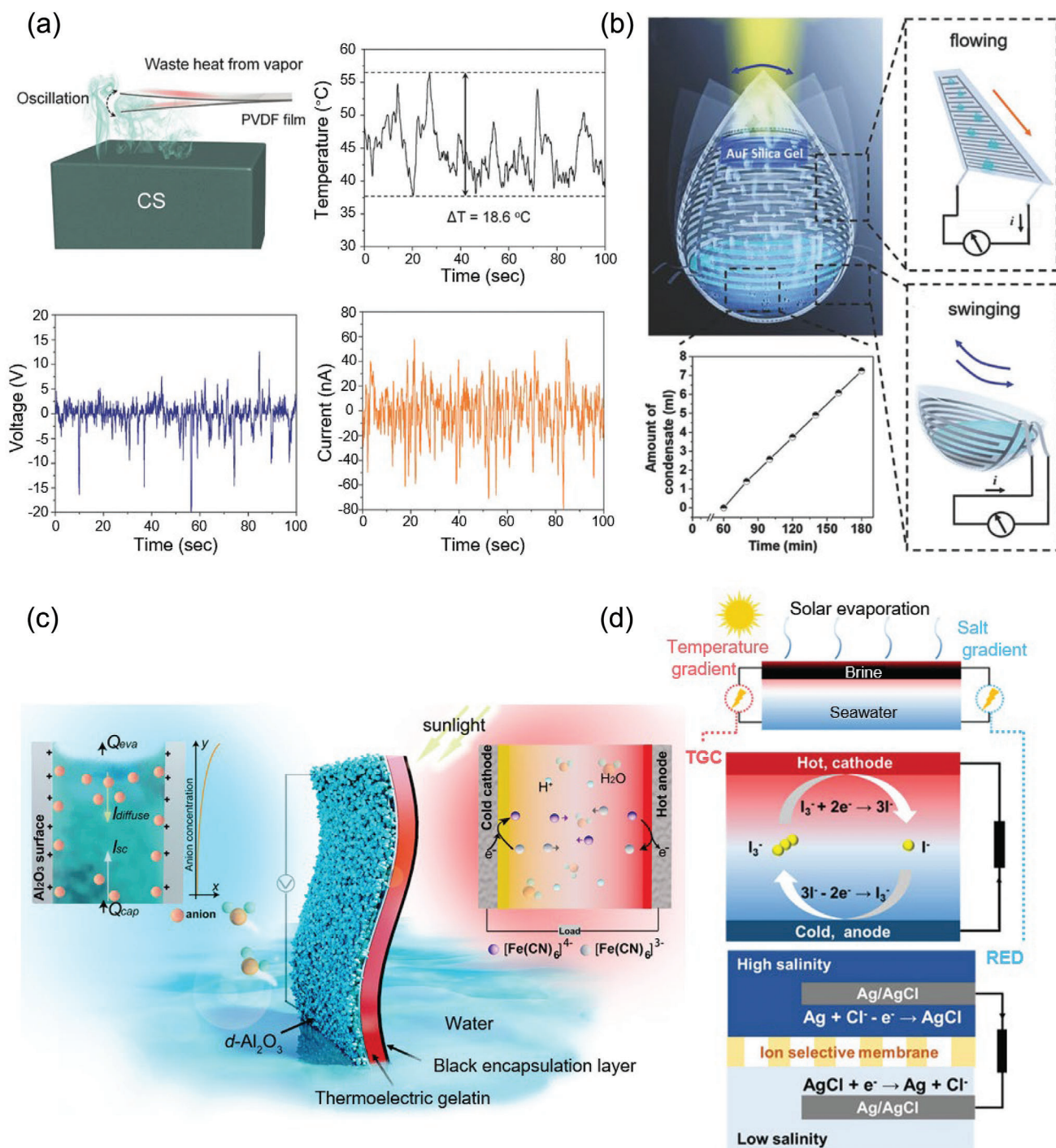


**Figure 6.** a) Schematic diagram of steam generation-induced electric potential of PVDF film with the corresponding temperature fluctuations, piezoelectric output currents and voltages. Reproduced with permission.<sup>[231]</sup> Copyright 2018, Wiley-VCH. b) Schematic diagram of the integral prototype for condensate collection and triboelectric energy generation of water flowing down the wall and water swinging in the round bottom vessel. Reproduced with permission.<sup>[232]</sup> Copyright 2018, Wiley-VCH. c) Schematic diagram and mechanism of the porous  $\text{Al}_2\text{O}_3$ -based hydrovoltaic generator integrated with flexible ionic thermolectric gelatine gel for sustained evaporation electricity output and thermolectric conversion. Reproduced with permission.<sup>[233]</sup> Copyright 2022, Springer Nature. d) A combination of thermogalvanic cell (TGC) and reverse electro dialysis (RED) technologies to generate electricity from temperature and salinity gradient during the solar-driven interfacial evaporation process. Reproduced with permission.<sup>[234]</sup> Copyright 2021, Wiley-VCH.

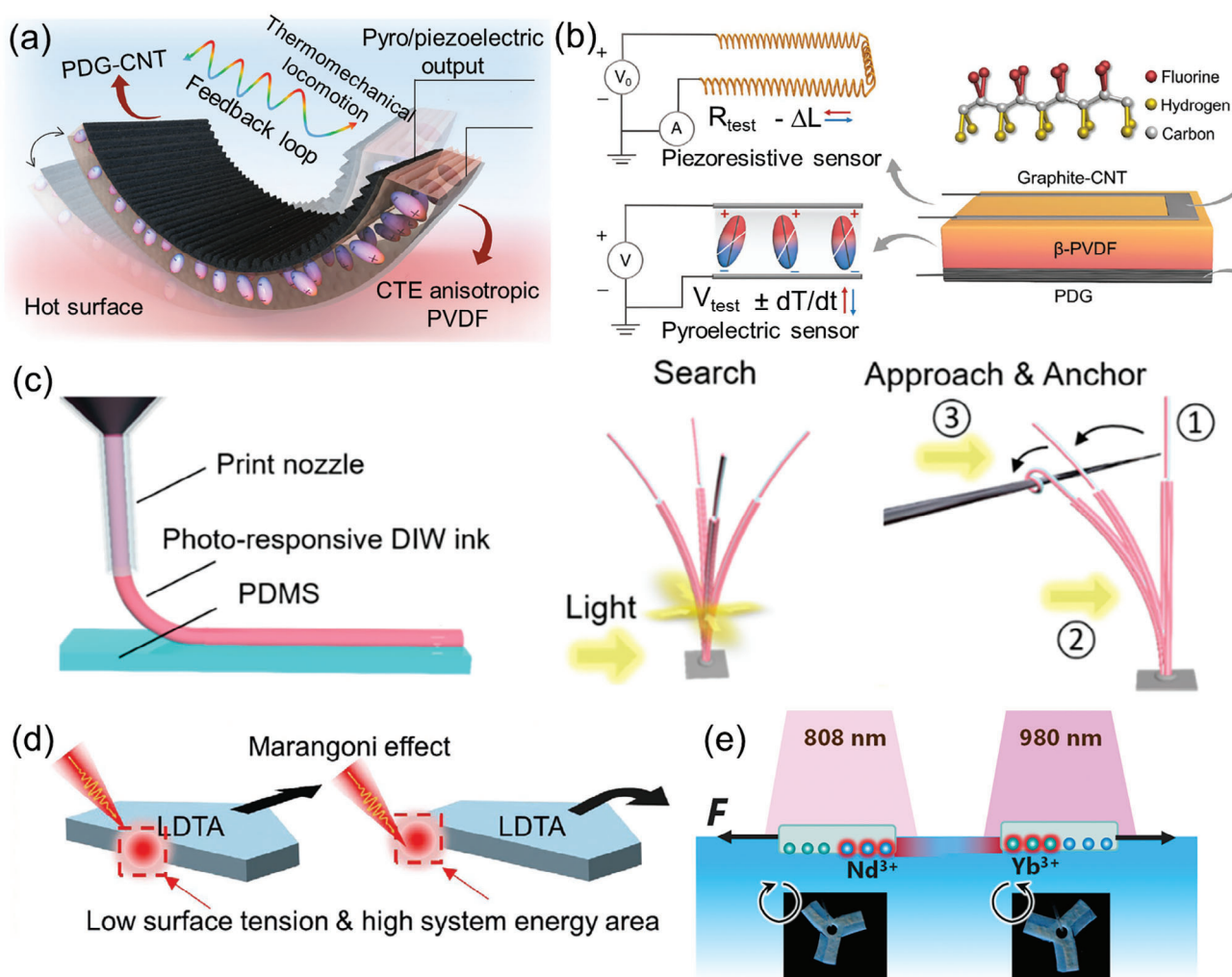


**Figure 7.** a) Design and concept of a PDG-CNT coated 3D-aligned ferroelectric PVDF film. Reproduced with permission.<sup>[238]</sup> Copyright 2018, Springer Nature. b) Materials system and working mechanism of light-driven actuator with self-powered temperature and strain sensing abilities. Reproduced with permission.<sup>[239]</sup> Copyright 2020, Wiley-VCH. c) Printing of NIPAM-based DIW ink (schematic), artificial tendrils demonstrating search behavior, and approach and anchor behavior. Reproduced with permission.<sup>[68]</sup> Copyright 2019, American Chemical Society. d) Schematic illustration of directional motions of LTMA induced by the Marangoni effect driven by NIR laser beam. Reproduced with permission.<sup>[244]</sup> Copyright 2021, Wiley-VCH. e) Three-bladed hydrogel propeller with  $Nd_2O_3$  and  $Yb_2O_3$  nanoparticles under 808 and 980 nm irradiation. Reproduced with permission.<sup>[249]</sup> Copyright 2021, American Chemical Society.

asymmetric thermal response of the PNIPAM–PDMS bilayer structure results in a bending deformation of the actuator. Artificial tendrils were then fabricated, and light was used to control and drive their bending motion, similar to the circumnutating motion of plant tendrils, demonstrating remote manipulation for tendril mimicry functions.

#### 4.3.2. Marangoni Propulsion

The Marangoni propulsion effect is a mass transport phenomenon commonly found in nature and is induced by the surface tension gradient on water. The gradient can be formed by photothermal heating where the surface tension of the irradiated area is lower than that of the nonirradiated area. With

this gradient, the liquid with high surface tension will exert a pulling force on the surrounding low surface tension liquid, and as long as a surface tension gradient is maintained by photothermal heating, there will be a continuous driving force for the actuators.<sup>[243]</sup>

A transparent light-driven 3D movable actuator (LTMA) was developed by embedding photothermal CuS nanoparticles in a PNIPAM hydrogel.<sup>[244]</sup> The CuS nanoparticles convert the absorbed light into heat which changes the surface energy of PNIPAM, leading to self-propulsion of the LTMA based on the Marangoni effect (Figure 7d). Moreover, the porous hydrogel can be engineered to sink/float by absorbing liquid molecules (sinking) and subsequently float by using a NIR laser beam to heat up the LTMA and generate a buoyant flow around it. Light-driven actuators using candle soot (CS) as the photothermal

material together with PDMS were also demonstrated. CS is a cheap and easily obtainable carbon material with a good photothermal conversion efficiency up to 57.5%, which is higher than some other photothermal materials such as gold nanorods (21%),<sup>[245]</sup> SnS nanosheets (36.1%)<sup>[246]</sup> and black phosphorus quantum dots (28.4%).<sup>[247]</sup> The use of a SU-8 mold enables the creation of actuators of various shapes and sizes, and the high transparency of PDMS allows the CS to receive light even if it is illuminated from the back side of the actuator. These actuators can perform linear, curvilinear and rotational movements via the Marangoni effect.<sup>[248]</sup> Besides this, an interesting concept of multimode motion of Marangoni propulsion ships on a water surface was also developed.<sup>[249]</sup> The direction of motion can be controlled by shining light of different wavelengths (808 or 980 nm) because two different types of photothermal materials ( $\text{Nd}_2\text{O}_3$  and  $\text{Yb}_2\text{O}_3$ ) were incorporated into the polyacrylamide or siloxane resin-based hydrogels at spatially separated locations (Figure 7e). The different photothermal responses of the materials to the specific light source enable selective localized heating of the gels without the need for deliberate positioning of the illumination. The temperature gradient of the ships generated by localized photothermal heating produces a Marangoni propulsion force in the desired direction.

In summary, photothermal hydrogels and membranes can be deployed as light-driven actuators with precise and remote control. PNIPAM hydrogel is a common choice because of its thermo-responsiveness, while inexpensive materials such as carbon can be used as the photothermal material. With continued development and improvements, these actuators have the potential to be used in future autonomous systems, further enhancing their utility and impact in various fields.

## 5. Challenges and Future Directions

In this review, the concept of photothermal effect has been introduced and the advantages and potential of photothermal hydrogels and membranes have been highlighted. The synthetic routes and considerations in materials design and engineering were summarized, and the application of hydrogels and membranes in clean water, fuel production, electricity generation, and mechanical actuator has also been discussed. Through these examples and discussions, it is evident that photothermal hydrogels and membranes exhibit more capabilities and can outperform their traditional counterparts in many of these applications. The achievements to date in this field have been significant, and much more exciting advancement is expected in coming years. However, there are some key challenges in the next phase of development, especially in the area of real-world deployment. To accelerate future progress, the following issues need to be addressed.

### 5.1. Artificial Intelligence Assisted Materials Exploration and Mechanism Understanding

Many materials have yet to be explored for use in photothermal hydrogels and membranes. Expanding the library of materials will enable the creation of hydrogels and membranes with new

functions or improved performance, serving a wider array of applications in various disciplines. Furthermore, the charge transport mechanism in hydrogels and membranes is still not fully understood. Hence, more in-depth investigations should be carried out in this area to facilitate design improvements that can further enhance energy conversion performance. Advanced or in situ characterizations, simulation and modeling can aid in understanding of these mechanisms. Artificial intelligence and machine learning can also be employed to run simulations to investigate and better understand the mechanisms behind the inclusion of the new materials. In this manner, it will be possible to find novel and optimal material compositions and improve the structural design of hydrogels and membranes.

### 5.2. Advanced Manufacturing

Additive manufacturing techniques such as 3D printing can be adopted to allow full customization and precise fabrication of photothermal specialized hydrogels and membranes with high throughput. In this way, complex shapes and nano/micro-sized structures can be created on the hydrogels and membranes for the enhancement of photothermal performance. The use of advanced manufacturing techniques also enables rapid fabrication and testing of photothermal samples, speeding up research efforts and output.

### 5.3. Large Scale Preparation for Practical Application

Despite showing better performance than their traditional counterparts, these photothermal hydrogels and membranes are mostly synthesized and tested in the lab. It is necessary to develop industrial scale production (e.g., roll-to-roll manufacturing) of these materials to realize commercial use and eventual industrial applications in our daily lives. Moreover, there is a significant gap between the current state-of-art and practical applications in various aspects of the technology development, including actual performance and long-term durability in the real-world environment. Therefore, more effort has to be made in designing systems suitable for actual deployment and long-term testing to demonstrate their true performance and capability.

### 5.4. Biodegradable Hydrogels and Membranes

In an effort to reduce waste, it might be possible to synthesize hydrogels and membranes from naturally abundant materials and sustainable materials such as cellulose, chitosan and alginate. Not only are these materials environmentally and biologically friendly, but they can also be recycled or biodegraded leaving little or no waste behind when it reaches the end of their useful life.

With these challenges well addressed, it can be expected that photothermal hydrogels and membranes of the future will bring about new scientific perspectives and new directions for practical applications, driving the evolution of photothermal materials and playing a critical role in achieving energy and environmental sustainability goals.

## Acknowledgements

This research was supported by A\*STAR, under its RIE2025 Manufacturing, Trade and Connectivity (MTC) Award Individual Research Grant (IRG award M22K2c0081) and the Ministry of Education, Singapore, under the Academic Research Fund Tier 1 (FY2023, A-8002151-00-00).

## Conflict of Interest

The authors declare no conflict of interest.

## Author Contributions

W.L.O. and W.L. contributed equally to this work. W.L.O., W.L. and T.Z. performed the investigation and wrote the original draft; G.W.H. conceptualized and supervised the study; W.L.O., W.L., T.Z. and G.W.H. wrote, reviewed, and edited the final draft. All authors have read and agreed to the published version of the manuscript.

## Keywords

actuators, electricity generation, hydrogen production, photothermal hydrogels/membranes, solar evaporation

Received: July 11, 2024

Revised: September 25, 2024

Published online: October 23, 2024

- [1] M. Gao, L. Zhu, C. K. Peh, G. W. Ho, *Energy Environ. Sci.* **2019**, *12*, 841.
- [2] L. Zhu, L. Tian, S. Jiang, L. Han, Y. Liang, Q. Li, S. Chen, *Chem. Soc. Rev.* **2023**, *52*, 7389.
- [3] T. Ding, Y. Zhou, W. L. Ong, G. W. Ho, *Mater. Today* **2021**, *42*, 178.
- [4] T. Ding, L. Zhu, X.-Q. Wang, K. H. Chan, X. Lu, Y. Cheng, G. W. Ho, *Adv. Energy Mater.* **2018**, *8*, 1802397.
- [5] W. Zhou, H. Huang, Y. Wu, J. Wang, Y. Yamauchi, J. Kim, S. M. Osman, X. Xu, L. Wang, C. Wang, Z. Yuan, *Chem. Eng. J.* **2023**, *471*, 144395.
- [6] H. Liu, H.-G. Ye, M. Gao, Q. Li, Z. Liu, A.-Q. Xie, L. Zhu, G. W. Ho, S. Chen, *Adv. Sci.* **2021**, *8*, 2101232.
- [7] L. Li, C. Xue, Q. Chang, X. Ren, N. Li, J. Yang, S. Hu, H. Xu, *Adv. Mater.* **2024**, *36*, 2401171.
- [8] C. Gao, Y. Li, L. Lan, Q. Wang, B. Zhou, Y. Chen, J. Li, J. Guo, J. Mao, *Adv. Sci.* **2024**, *11*, 2306833.
- [9] Y. Zhao, C.-Y. Lo, L. Ruan, C.-H. Pi, C. Kim, Y. Alsaied, I. Frenkel, R. Rico, T.-C. Tsao, X. He, *Sci. Rob.* **2021**, *6*, eabd5483.
- [10] Y. Yang, Y. Liu, Y. Shen, *Adv. Funct. Mater.* **2020**, *30*, 1910172.
- [11] C. Zhang, H.-Q. Liang, Z.-K. Xu, Z. Wang, *Adv. Sci.* **2019**, *6*, 1900883.
- [12] C. Ma, J. Yan, Y. Huang, C. Wang, G. Yang, *Sci. Adv.* **2018**, *4*, eaas9894.
- [13] P. Cheng, D. Wang, P. Schaaf, *Adv. Sustainable Syst.* **2022**, *6*, 2200115.
- [14] J.-W. Xu, K. Yao, Z.-K. Xu, *Nanoscale* **2019**, *11*, 8680.
- [15] H. K. Moon, S. H. Lee, H. C. Choi, *ACS Nano* **2009**, *3*, 3707.
- [16] Y. Lin, H. Xu, X. Shan, Y. Di, A. Zhao, Y. Hu, Z. Gan, *J. Mater. Chem. A* **2019**, *7*, 19203.
- [17] M. Gao, T. Zhang, G. W. Ho, *Nano Res.* **2022**, *15*, 9985.
- [18] M.-Q. Yang, M. Gao, M. Hong, G. W. Ho, *Adv. Mater.* **2018**, *30*, 1802894.
- [19] L. Zhu, M. Gao, C. K. N. Peh, G. W. Ho, *Mater. Horiz.* **2018**, *5*, 323.
- [20] M. Gao, P. K. N. Connor, G. W. Ho, *Energy Environ. Sci.* **2016**, *9*, 3151.
- [21] M. Gao, C. K. Peh, F. L. Meng, G. W. Ho, *Small Methods* **2021**, *5*, 2001200.
- [22] A. Politano, P. Argurio, G. Di Profio, V. Sanna, A. Cupolillo, S. Chakraborty, H. A. Arafat, E. Curcio, *Adv. Mater.* **2017**, *29*, 1603504.
- [23] M. Gao, C. K. Peh, L. Zhu, G. Yilmaz, G. W. Ho, *Adv. Energy Mater.* **2020**, *10*, 2000925.
- [24] C. Li, B. Zhu, Z. Liu, J. Zhao, R. Meng, L. Zhang, Z. Chen, *Chem. Eng. J.* **2022**, *431*, 134224.
- [25] S. Chen, F. Tang, L. Tang, L. Li, *ACS Appl. Mater. Interfaces* **2017**, *9*, 20895.
- [26] G. Xie, X. Wang, M. Mo, L. Zhang, J. Zhu, *Macromol. Biosci.* **2023**, *23*, 2200378.
- [27] Y. S. Zhang, A. Khademhosseini, *Science* **2017**, *356*, eaaf3627.
- [28] E. M. Ahmed, *J. Adv. Res.* **2015**, *6*, 105.
- [29] X. Liu, J. Liu, S. Lin, X. Zhao, *Mater. Today* **2020**, *36*, 102.
- [30] D. Yang, *Chem. Mater.* **1987**, *34*.
- [31] C. Zhou, D. E. Heath, A. R. M. Sharif, S. Rayatpisheh, B. H. L. Oh, X. Rong, R. Beuerman, M. B. Chan-Park, *Macromol. Biosci.* **2013**, *13*, 1485.
- [32] Y. Huang, M. Zhang, W. Ruan, *J. Mater. Chem. A* **2014**, *2*, 10508.
- [33] X. N. Zhang, Y. J. Wang, S. Sun, L. Hou, P. Wu, Z. L. Wu, Q. Zheng, *Macromolecules* **2018**, *51*, 8136.
- [34] X. Bai, S. Lü, Z. Cao, C. Gao, H. Duan, X. Xu, L. Sun, N. Gao, C. Feng, M. Liu, *Chem. Eng. J.* **2016**, *288*, 546.
- [35] C. Chang, B. Duan, J. Cai, L. Zhang, *Eur. Polym. J.* **2010**, *46*, 92.
- [36] Q. Lv, M. Wu, Y. Shen, *Colloids Surf., A* **2019**, *583*, 123972.
- [37] C. Yang, Z. Suo, *Nat. Rev. Mater.* **2018**, *3*, 125.
- [38] H. Yuk, B. Lu, X. Zhao, *Chem. Soc. Rev.* **2019**, *48*, 1642.
- [39] Y. Zhou, C. Wan, Y. Yang, H. Yang, S. Wang, Z. Dai, K. Ji, H. Jiang, X. Chen, Y. Long, *Adv. Funct. Mater.* **2019**, *29*, 1806220.
- [40] L. Hu, P. L. Chee, S. Sugiarto, Y. Yu, C. Shi, R. Yan, Z. Yao, X. Shi, J. Zhi, D. Kai, H.-D. Yu, W. Huang, *Adv. Mater.* **2023**, *35*, 2205326.
- [41] O. Okay, in *Hydrogel Sensors and Actuators: Engineering and Technology* (Eds.: G. Gerlach, K.-F. Arndt), Springer, Berlin **2010**, p. 1.
- [42] B. Kaczmarek, K. Nadolna, A. Owczarek, in *Hydrogels Based on Natural Polymers* (Ed.: Y. Chen), Elsevier, Amsterdam **2020**, p. 151.
- [43] Y. Guo, L. S. de Vasconcelos, N. Manohar, J. Geng, K. P. Johnston, G. Yu, *Angew. Chem., Int. Ed.* **2022**, *61*, 202114074.
- [44] T. Gancheva, N. Virgilio, *Macromolecules* **2016**, *49*, 5866.
- [45] Y. Alsaied, S. Wu, D. Wu, Y. Du, L. Shi, R. Khodambashi, R. Rico, M. Hua, Y. Yan, Y. Zhao, D. Aukes, X. He, *Adv. Mater.* **2021**, *33*, 2008235.
- [46] H. Liu, M. Li, S. Liu, P. Jia, X. Guo, S. Feng, T. J. Lu, H. Yang, F. Li, F. Xu, *Mater. Horiz.* **2020**, *7*, 203.
- [47] L. Tang, S. Wu, J. Qu, L. Gong, J. Tang, *Materials* **2020**, *13*, 3947.
- [48] W. Lu, T. Ding, X. Wang, C. Zhang, T. Li, K. Zeng, G. W. Ho, *Nano Energy* **2022**, *104*, 107892.
- [49] M. Wu, J. Chen, Y. Ma, B. Yan, M. Pan, Q. Peng, W. Wang, L. Han, J. Liu, H. Zeng, *J. Mater. Chem. A* **2020**, *8*, 24718.
- [50] H. Tian, C. Wang, Y. Chen, L. Zheng, H. Jing, L. Xu, X. Wang, Y. Liu, J. Hao, *Sci. Adv.* **2023**, *9*, eadd6950.
- [51] M. Vázquez-González, I. Willner, *Angew. Chem., Int. Ed.* **2020**, *59*, 15342.
- [52] P. Zarrintaj, S. Manouchehri, Z. Ahmadi, M. R. Saeb, A. M. Urbanska, D. L. Kaplan, M. Mozafari, *Carbohydr. Polym.* **2018**, *187*, 66.
- [53] S. P. Miguel, M. P. Ribeiro, H. Brancal, P. Coutinho, I. J. Correia, *Carbohydr. Polym.* **2014**, *111*, 366.
- [54] A. Saarai, T. Sedlacek, V. Kasparkova, T. Kitano, P. Saha, *J. Appl. Polym. Sci.* **2012**, *126*, E79.
- [55] M. C. G. Pellá, M. K. Lima-Tenório, E. T. Tenório-Neto, M. R. Guilherme, E. C. Muniz, A. F. Rubira, *Carbohydr. Polym.* **2018**, *196*, 233.

- [56] Y. Zhou, T. Ding, M. Gao, K. H. Chan, Y. Cheng, J. He, G. W. Ho, *Nano Energy* **2020**, *77*, 105102.
- [57] F. L. Meng, M. Gao, T. Ding, G. Yilmaz, W. L. Ong, G. W. Ho, *Adv. Funct. Mater.* **2020**, *30*, 2002867.
- [58] M. Wang, J. Bai, K. Shao, W. Tang, X. Zhao, D. Lin, S. Huang, C. Chen, Z. Ding, J. Ye, *Int. J. Polym. Sci.* **2021**, *2021*, 2225426.
- [59] X.-Q. Wang, K. H. Chan, W. Lu, T. Ding, S. W. L. Ng, Y. Cheng, T. Li, M. Hong, B. C. K. Tee, G. W. Ho, *Nat. Commun.* **2022**, *13*, 3369.
- [60] B. C. Pattnayak, S. Mohapatra, *J. Environ. Chem. Eng.* **2022**, *10*, 108616.
- [61] J. He, M. Shi, Y. Liang, B. Guo, *Chem. Eng. J.* **2020**, *394*, 124888.
- [62] C.-H. Zhu, Y. Lu, J. Peng, J.-F. Chen, S.-H. Yu, *Adv. Funct. Mater.* **2012**, *22*, 4017.
- [63] Y. Bai, Y. Lu, S. Bi, W. Wang, F. Lin, F. Zhu, P. Yang, N. Ding, S. Liu, W. Zhao, N. Liu, Q. Zhao, *Adv. Mater. Technol.* **2023**, *8*, 2201767.
- [64] T. Ding, K. H. Chan, Y. Zhou, X.-Q. Wang, Y. Cheng, T. Li, G. W. Ho, *Nat. Commun.* **2020**, *11*, 6006.
- [65] M. Hua, S. Wu, Y. Ma, Y. Zhao, Z. Chen, I. Frenkel, J. Strzalka, H. Zhou, X. Zhu, X. He, *Nature* **2021**, *590*, 594.
- [66] J. Li, K. Pan, H. Tian, L. Yin, *Macromol. Mater. Eng.* **2020**, *305*, 2000285.
- [67] G. Chen, G. Wang, X. Tan, K. Hou, Q. Meng, P. Zhao, S. Wang, J. Zhang, Z. Zhou, T. Chen, Y. Cheng, B. S. Hsiao, E. Reichmanis, M. Zhu, *Natl. Sci. Rev.* **2020**, *8*, nwaa209.
- [68] Y. Cheng, K. H. Chan, X.-Q. Wang, T. Ding, T. Li, X. Lu, G. W. Ho, *ACS Nano* **2019**, *13*, 13176.
- [69] Y. Dong, S. Wang, Y. Ke, L. Ding, X. Zeng, S. Magdassi, Y. Long, *Adv. Mater. Technol.* **2020**, *5*, 2000034.
- [70] M. Champeau, D. A. Heinze, T. N. Viana, E. R. de Souza, A. C. Chinellato, S. Titotto, *Adv. Funct. Mater.* **2020**, *30*, 1910606.
- [71] Y. Huang, X. Li, Z. Lu, H. Zhang, J. Huang, K. Yan, D. Wang, *J. Mater. Chem. B* **2020**, *8*, 9794.
- [72] Y. Zhang, T. Ma, F. Zhang, W. Guo, K. Yu, C. Yang, F. Qu, *J. Colloid Interface Sci.* **2022**, *607*, 1446.
- [73] X. Xu, R. M. Sarhan, S. Mei, Z. Kochovski, W. Koopman, R. D. Priestley, Y. Lu, *ACS Appl. Mater. Interfaces* **2023**, *15*, 48623.
- [74] N. Abdullah, M. A. Rahman, M. H. Dzarfan Othman, J. Jaafar, A. F. Ismail, in *Current Trends and Future Developments on (Bio-) Membranes* (Eds.: A. Basile, S. Mozia, R. Molinari), Elsevier, Amsterdam **2018**, pp. 45.
- [75] H. M. Saleh, A. I. Hassan, *Green Energy Environ. Technol.* **2022**, <https://doi.org/10.5772/geet.01>.
- [76] H. Watson, *Essays Biochem.* **2015**, *59*, 43.
- [77] A. Deshmukh, C. Boo, V. Karanikola, S. Lin, A. P. Straub, T. Tong, D. M. Warsinger, M. Elimelech, *Energy Environ. Sci.* **2018**, *11*, 1177.
- [78] E. Drioli, E. Fontananova, *Annu. Rev. Chem. Biomol. Eng.* **2012**, *3*, 395.
- [79] X. He, M.-B. Hägg, *Membranes* **2012**, *2*, 706.
- [80] P. Vadgama, *J. Membr. Sci.* **1990**, *50*, 141.
- [81] N. Du, H. B. Park, M. M. Dal-Cin, M. D. Guiver, *Energy Environ. Sci.* **2012**, *5*, 7306.
- [82] J. Xie, Z. Liao, M. Zhang, L. Ni, J. Qi, C. Wang, X. Sun, L. Wang, S. Wang, J. Li, *Environ. Sci. Technol.* **2021**, *55*, 2652.
- [83] B. S. Lalia, V. Kochkodan, R. Hashaiekh, N. Hilal, *Desalination* **2013**, *326*, 77.
- [84] M. U. Siddiqui, A. F. M. Arif, S. Bashmal, *Membranes* **2016**, *6*, 40.
- [85] B. Gu, D. L. Renaud, P. Sanaei, L. Kondic, L. J. Cummings, *J. Fluid Mech.* **2020**, *902*, A5.
- [86] Y. Wang, Q. Jiang, W. Jing, Z. Zhong, W. Xing, *J. Membr. Sci.* **2022**, *648*, 120347.
- [87] F. Li, Y. Yang, Y. Fan, W. Xing, Y. Wang, *J. Membr. Sci.* **2012**, *397*, 17.
- [88] R. M. DuChanois, R. Epszstein, J. A. Trivedi, M. Elimelech, *J. Membr. Sci.* **2019**, *581*, 413.
- [89] S. Rangou, K. Buhr, V. Filiz, J. I. Clodt, B. Lademann, J. Hahn, A. Jung, V. Abetz, *J. Membr. Sci.* **2014**, *451*, 266.
- [90] D. L. Shaffer, H. Jaramillo, S. Romero-Vargas Castrillón, X. Lu, M. Elimelech, *J. Membr. Sci.* **2015**, *490*, 209.
- [91] E. Shauly, S. Nejadi, C. Boo, F. Perreault, C. O. Osuji, M. Elimelech, *J. Membr. Sci.* **2017**, *530*, 158.
- [92] A. Tufani, G. O Ince, *J. Membr. Sci.* **2017**, *537*, 255.
- [93] Z. Zhang, X. Xiao, Y. Zhou, L. Huang, Y. Wang, Q. Rong, Z. Han, H. Qu, Z. Zhu, S. Xu, J. Tang, J. Chen, *ACS Nano* **2021**, *15*, 13178.
- [94] W. Pu, X. He, L. Wang, C. Jiang, C. Wan, *J. Membr. Sci.* **2006**, *272*, 11.
- [95] X. Lu, M. Elimelech, *Chem. Soc. Rev.* **2021**, *50*, 6290.
- [96] V. Hornok, A. Erdőhelyi, I. Dékány, *Colloid. Polym. Sci.* **2006**, *284*, 611.
- [97] F. E. Ahmed, B. S. Lalia, R. Hashaiekh, *Desalination* **2015**, *356*, 15.
- [98] N. Agoudjil, S. Kermadi, A. Larbot, *Desalination* **2008**, *223*, 417.
- [99] R. Vinoth Kumar, A. Kumar Ghoshal, G. Pugazhenthii, *J. Membr. Sci.* **2015**, *490*, 92.
- [100] K. Wang, D. Hou, J. Wang, Z. Wang, B. Tian, P. Liang, *Appl. Surf. Sci.* **2018**, *450*, 57.
- [101] P. van Rijn, M. Tutus, C. Kathrein, L. Zhu, M. Wessling, U. Schwaneberg, A. Böker, *Chem. Soc. Rev.* **2013**, *42*, 6578.
- [102] Y. Ju, J. Zhang, Q. Cai, Z. Zhang, Y. Zhao, J. Cui, R. Hou, Y. Wei, Z. Liang, F. Chen, *Chem. Eng. J.* **2023**, *453*, 139969.
- [103] S. Kim, H. Wang, Y. M. Lee, *Angew. Chem., Int. Ed.* **2019**, *58*, 17512.
- [104] C. Zhang, W. Lu, Y. Xu, K. Zeng, G. W. Ho, *Nature* **2023**, *616*, 293.
- [105] W. Cai, S. Zhao, K. Zhang, K. Guo, Y. Wang, Q. Chen, Y. Wang, *Ind. Eng. Chem. Res.* **2023**, *62*, 10175.
- [106] B. Zhang, H. Luo, B. Ai, Q. Gou, J. Deng, J. Wang, Y. Zheng, J. Xiao, M. Li, *Small* **2023**, *19*, 2205431.
- [107] X. Liu, X. Jin, L. Li, J. Wang, Y. Yang, Y. Cao, W. Wang, *J. Mater. Chem. A* **2020**, *8*, 12526.
- [108] L. Shi, Y. Shi, C. Zhang, S. Zhuo, W. Wang, R. Li, P. Wang, *Energy Technol.* **2020**, *8*, 2000456.
- [109] J. Liu, A. Moreno, J. Chang, M. Morsali, J. Yuan, M. H. Sipponen, *ACS Appl. Mater. Interfaces* **2022**, *14*, 12693.
- [110] S. Wang, J. Lin, Y. He, J. Chen, C. Yang, F. Huang, D. Chen, *Chem. Eng. J.* **2020**, *394*, 124889.
- [111] K. MUSAIE, S. Abbaszadeh, V. Nosrati-Siahmazgi, M. Qahremani, S. Wang, M. R. Eskandari, S. V. Niknezhad, F. Haghi, Y. Li, B. Xiao, M.-A. Shahbazi, *Biomater. Sci.* **2023**, *11*, 2486.
- [112] P.-P. He, X. Du, Y. Cheng, Q. Gao, C. Liu, X. Wang, Y. Wei, Q. Yu, W. Guo, *Small* **2022**, *18*, 2200263.
- [113] L. Zhang, L. Chen, L. Xu, H. Zhao, R. Wen, F. Xia, *Adv. Mater.* **2023**, *35*, 2212149.
- [114] H.-C. Yang, F. Lu, H.-N. Li, C. Zhang, S. B. Darling, Z.-K. Xu, *Adv. Funct. Mater.* **2023**, *33*, 2304580.
- [115] S. Ding, T. Zhang, M. Wu, X. Wang, *J. Membr. Sci.* **2023**, *680*, 121740.
- [116] W. Lu, W. L. Ong, G. W. Ho, *J. Mater. Chem. A* **2023**, *11*, 12456.
- [117] W. Pei, Z. Xie, X. Pei, J. Wang, *Chem. Eng. J.* **2024**, *495*, 153420.
- [118] Z. Zhang, X. Li, J. Yin, Y. Xu, W. Fei, M. Xue, Q. Wang, J. Zhou, W. Guo, *Nat. Nanotechnol.* **2018**, *13*, 1109.
- [119] X. Tong, S. Liu, J. Crittenden, Y. Chen, *ACS Nano* **2021**, *15*, 5838.
- [120] B. Zhang, P. W. Wong, A. K. An, *Chem. Eng. J.* **2022**, *430*, 133054.
- [121] J. Sun, M. U. Farid, M. W. Boey, Y. Sato, G. Chen, A. K. An, *Chem. Eng. J.* **2023**, *468*, 143744.
- [122] Y. Liu, F. Li, Z. Guo, Y. Xiao, Y. Zhang, X. Sun, T. Zhe, Y. Cao, L. Wang, Q. Lu, J. Wang, *Chem. Eng. J.* **2020**, *382*, 122990.
- [123] X. Zhang, B. Tan, Y. Wu, M. Zhang, J. Liao, *Polymers* **2021**, *13*, 2100.
- [124] Y. Min, R. Han, G. Li, X. Wang, S. Chen, M. Xie, Z. Zhao, *Adv. Funct. Mater.* **2023**, *33*, 2212803.
- [125] X. Ma, J. Zhao, D. Shou, Y. Liu, *Adv. Energy Mater.* **2024**, *14*, 2304032.
- [126] X. Shi, L. Ma, Y. Li, Z. Shi, Q. Wei, G. Ma, W. Zhang, Y. Guo, P. Wu, Z. Hu, *Adv. Funct. Mater.* **2023**, *33*, 2211720.

- [127] X. Yuan, J. Zhang, J. Shi, W. Liu, A. S. Kritchenkov, S. Van Vlierberghe, L. Wang, W. Liu, J. Gao, *Polymers* **2024**, *16*, 1346.
- [128] Q. Yan, B. Xin, Z. Chen, Y. Liu, *Mater. Today Commun.* **2021**, *28*, 102584.
- [129] J. Wang, Y. Cao, B. Jaquet, C. Gerhard, W. Li, X. Xia, J. E. Rauschendorfer, P. Vana, K. Zhang, *ACS Appl. Mater. Interfaces* **2021**, *13*, 28668.
- [130] D. Zheng, L. Shi, M. Zhang, W. Jiang, C. An, W. Huang, H. Fei, C. Zhang, *J. Environ. Chem. Eng.* **2024**, *12*, 112004.
- [131] M. Kim, J.-H. Lee, J.-M. Nam, *Adv. Sci.* **2019**, *6*, 1900471.
- [132] K. W. Tan, C. M. Yap, Z. Zheng, C. Y. Haw, P. S. Khiew, W. S. Chiu, *Adv. Sustain. Syst.* **2022**, *6*, 2100416.
- [133] C. Tan, L. Zhao, P. Yu, Y. Huang, B. Chen, Z. Lai, X. Qi, M. H. Goh, X. Zhang, S. Han, X.-J. Wu, Z. Liu, Y. Zhao, H. Zhang, *Angew. Chem., Int. Ed.* **2017**, *56*, 7842.
- [134] P. Liu, X.-Y. Li, L. Xu, C. Chen, B. Yuan, L. Labiadh, Y.-b. Hu, M.-L. Fu, *Desalination* **2022**, *527*, 115532.
- [135] B. Han, Y.-L. Zhang, Q.-D. Chen, H.-B. Sun, *Adv. Funct. Mater.* **2018**, *28*, 1802235.
- [136] Y. Li, Y. Shi, H. Wang, T. Liu, X. Zheng, S. Gao, J. Lu, *Carbon Energy* **2023**, *5*, e331.
- [137] D. Xu, Z. Li, L. Li, J. Wang, *Adv. Funct. Mater.* **2020**, *30*, 2000712.
- [138] L. Xu, L. Cheng, C. Wang, R. Peng, Z. Liu, *Polym. Chem.* **2014**, *5*, 1573.
- [139] Y. Lyu, C. Xie, S. A. Chechetka, E. Miyako, K. Pu, *J. Am. Chem. Soc.* **2016**, *138*, 9049.
- [140] S. Lv, Y. Miao, D. Liu, F. Song, *ChemBioChem* **2020**, *21*, 2098.
- [141] J. Huang, Y. He, M. Chen, B. Jiang, Y. Huang, *Sol. Energy* **2017**, *155*, 1225.
- [142] A. Guo, Y. Fu, G. Wang, X. Wang, *RSC Adv.* **2017**, *7*, 4815.
- [143] G. Yilmaz, F. L. Meng, W. Lu, J. Abed, C. K. N. Peh, M. Gao, E. H. Sargent, G. W. Ho, *Sci. Adv.* **2020**, *6*, eabc8605.
- [144] S. W. L. Ng, M. Gao, W. Lu, M. Hong, G. W. Ho, *Adv. Funct. Mater.* **2021**, *31*, 2104750.
- [145] Y. Shi, C. Zhang, Y. Wang, Y. Cui, Q. Wang, G. Liu, S. Gao, Y. Yuan, *Desalination* **2021**, *507*, 115038.
- [146] H. Zhang, J. Ou, X. Fang, S. Lei, F. Wang, C. Li, W. Li, Y. Hu, A. Amirfazli, P. Wang, *Chem. Eng. J.* **2022**, *429*, 132539.
- [147] C. H. Liow, X. Lu, K. Zeng, S. Li, G. W. Ho, *Small* **2019**, *15*, 1903042.
- [148] S.-C. Cai, J.-J. Li, E.-Q. Yu, X. Chen, J. Chen, H.-P. Jia, *ACS Appl. Nano Mater* **2018**, *1*, 6368.
- [149] E. Petryayeva, U. J. Krull, *Anal. Chim. Acta* **2011**, *706*, 8.
- [150] J. Boken, P. Khurana, S. Thatai, D. Kumar, S. Prasad, *Appl. Spectrosc. Rev.* **2017**, *52*, 774.
- [151] R. Long, Y. Li, L. Song, Y. Xiong, *Small* **2015**, *11*, 3873.
- [152] E. Ye, K. Y. Win, H. R. Tan, M. Lin, C. P. Teng, A. Mlayah, M.-Y. Han, *J. Am. Chem. Soc.* **2011**, *133*, 8506.
- [153] Z. Li, H. Li, S. Wang, F. Yang, W. Zhou, *Chem. Eng. J.* **2022**, *427*, 131830.
- [154] J. Fang, Y. Xuan, *RSC Adv.* **2017**, *7*, 56023.
- [155] C. Shi, D. Yuan, L. Ma, Y. Li, Y. Lu, L. Gao, X. San, S. Wang, G. Fu, *J. Mater. Chem. A* **2020**, *8*, 19467.
- [156] Y. Zhong, C. Wu, Y. Feng, D. Chen, Y. Wang, D. Hao, H. Ding, *Appl. Surf. Sci.* **2022**, *585*, 152656.
- [157] D. Sun, J. Cai, Y. Yang, Z. Liang, *Chem. Eng. Sci.* **2024**, *284*, 119454.
- [158] Q. Tian, M. Tang, Y. Sun, R. Zou, Z. Chen, M. Zhu, S. Yang, J. Wang, J. Wang, J. Hu, *Adv. Mater.* **2011**, *23*, 3542.
- [159] Z. Hua, B. Li, L. Li, X. Yin, K. Chen, W. Wang, *J. Phys. Chem. C* **2017**, *121*, 60.
- [160] Z. Xie, Y. Duo, Z. Lin, T. Fan, C. Xing, L. Yu, R. Wang, M. Qiu, Y. Zhang, Y. Zhao, X. Yan, H. Zhang, *Adv. Sci.* **2020**, *7*, 1902236.
- [161] Z. Li, H. Lei, A. Kan, H. Xie, W. Yu, *Energy* **2021**, *216*, 119262.
- [162] S. Loeb, C. Li, J.-H. Kim, *Environ. Sci. Technol.* **2018**, *52*, 205.
- [163] G. Liu, J. Xu, K. Wang, *Nano Energy* **2017**, *41*, 269.
- [164] Y. Gogotsi, B. Anasori, *ACS Nano* **2019**, *13*, 8491.
- [165] Z. Wang, Y. Yan, X. Shen, C. Jin, Q. Sun, H. Li, *J. Mater. Chem. A* **2019**, *7*, 20706.
- [166] Q. Zhao, Y. Wan, F. Chang, Y. Wang, H. Jiang, L. Jiang, X. Zhang, N. Ma, *Desalination* **2022**, *527*, 115581.
- [167] J.-W. Li, Y. Zhou, J. Xu, F. Gao, Q.-K. Si, J.-Y. Wang, F. Zhang, L.-P. Wang, *ACS Appl. Mater. Interfaces* **2022**, *14*, 52670.
- [168] M. Zangoli, F. Di Maria, *VIEW* **2021**, *2*, 20200086.
- [169] B. Poinard, S. Z. Y. Neo, E. L. L. Yeo, H. P. S. Heng, K. G. Neoh, J. C. Y. Kah, *ACS Appl. Mater. Interfaces* **2018**, *10*, 21125.
- [170] L. Li, X. Han, M. Wang, C. Li, T. Jia, X. Zhao, *Chem. Eng. J.* **2021**, *417*, 128844.
- [171] Q. Jiang, D. Ghim, S. Cao, S. Tadepalli, K.-K. Liu, H. Kwon, J. Luan, Y. Min, Y.-S. Jun, S. Singamaneni, *Environ. Sci. Technol.* **2019**, *53*, 412.
- [172] C. Liu, P. Wu, *RSC Adv.* **2024**, *14*, 10370.
- [173] Q. Luo, P. Liu, L. Fu, Y. Hu, L. Yang, W. Wu, X.-Y. Kong, L. Jiang, L. Wen, *ACS Appl. Mater. Interfaces* **2022**, *14*, 13223.
- [174] N. Zhang, J. Zhang, X. Zhu, S. Yuan, D. Wang, H. Xu, Z. Wang, *Nano Lett.* **2024**, *24*, 724.
- [175] G. Xie, N. Zhou, S. Du, Y. Gao, H. Suo, J. Yang, J. Tao, J. Zhu, L. Zhang, *Fundam. Res.* **2021**, *2*, 268.
- [176] W. Li, L. Deng, H. Huang, J. Zhou, Y. Liao, L. Qiu, H. Yang, L. Yao, *ACS Appl. Mater. Interfaces* **2021**, *13*, 26861.
- [177] Y. Liu, X. Zheng, *Sol. Energy* **2024**, *273*, 112507.
- [178] X. Guo, H. Gao, S. Wang, L. Yin, Y. Dai, *Desalination* **2020**, *488*, 114535.
- [179] B. Zhang, P. W. Wong, J. Guo, Y. Zhou, Y. Wang, J. Sun, M. Jiang, Z. Wang, A. K. An, *Nat. Commun.* **2022**, *13*, 3315.
- [180] Y. Lu, D. Fan, Y. Wang, H. Xu, C. Lu, X. Yang, *ACS Nano* **2021**, *15*, 10366.
- [181] F. Xu, D. Weng, X. Li, Y. Li, J. Sun, *CCS Chem.* **2022**, *4*, 2396.
- [182] T. Kuckhoff, K. Landfester, K. A. I. Zhang, C. T. J. Ferguson, *Chem. Mater.* **2021**, *33*, 9131.
- [183] H. Heidarpour, M. Golizadeh, M. Padervand, A. Karimi, M. Vossoughi, M. H. Tavakoli, *J. Photochem. Photobiol. A* **2020**, *398*, 112559.
- [184] C. Ma, Z. Xie, W. C. Seo, S. T. Ud Din, J. Lee, Y. Kim, H. Jung, W. Yang, *Appl. Surf. Sci.* **2021**, *565*, 150564.
- [185] L. Lei, W. Wang, C. Wang, H. Fan, A. K. Yadav, N. Hu, Q. Zhong, P. Müller-Buschbaum, *J. Mater. Chem. A* **2020**, *8*, 23812.
- [186] Y. Zhang, N. Zhang, Y. Liu, Y. Chen, H. Huang, W. Wang, X. Xu, Y. Li, F. Fan, J. Ye, Z. Li, Z. Zou, *Nat. Commun.* **2022**, *13*, 2942.
- [187] C. Qin, W. Wu, H. Goma, S. Wu, C. An, Q. Deng, N. Hu, *J. Energy Chem.* **2023**, *86*, 518.
- [188] J. Schlenkrich, F. Lubkemann-Warwas, R. T. Graf, C. Wesemann, L. Schoske, M. Rosebrock, K. D. J. Hindricks, P. Behrens, D. W. Bahnemann, D. Dorfs, N. C. Bigall, *Small* **2023**, *19*, 2208108.
- [189] M. Q. Yang, C. F. Tan, W. Lu, K. Zeng, G. W. Ho, *Adv. Funct. Mater.* **2020**, *30*, 2004460.
- [190] P. Chen, Q. Ruan, R. Nasser, H. Zhang, X. Xi, H. Xia, G. Xu, Q. Xie, C. Yi, Z. Sun, H. Shahsavan, W. Zhang, *Adv. Sci.* **2022**, *9*, 2204730.
- [191] W. H. Lee, C. W. Lee, G. D. Cha, B. H. Lee, J. H. Jeong, H. Park, J. Heo, M. S. Bootharaju, S. H. Sunwoo, J. H. Kim, K. H. Ahn, D. H. Kim, T. Hyeon, *Nat. Nanotechnol.* **2023**, *18*, 754.
- [192] P. Lin, X. Qu, B. J. Deka, C. Hu, L. Zhao, D. Wu, C. Yi, M. W. Boey, M. U. Farid, A. K. An, J. Guo, *Chem. Eng. J.* **2024**, *489*, 151268.
- [193] D. Lou, A.-B. Xu, Y. Fang, M. Cai, K. Lv, D. Zhang, X. Wang, Y. Huang, C. Li, L. He, *ChemNanoMat* **2021**, *7*, 1008.
- [194] Y. Tian, X. Liu, S. Xu, J. Li, A. Caratenuto, Y. Mu, Z. Wang, F. Chen, R. Yang, J. Liu, M. L. Minus, Y. Zheng, *Desalination* **2022**, *523*, 115449.

- [195] X. Xu, S. Ozden, N. Bizmark, C. B. Arnold, S. S. Datta, R. D. Priestley, *Adv. Mater.* **2021**, *33*, 2007833.
- [196] A. Ni, D. Fu, P. Lin, X. Wang, Y. Xia, X. Han, T. Zhang, *J. Colloid Interface Sci.* **2023**, *647*, 344.
- [197] Y. S. Jun, X. Wu, D. Ghim, Q. Jiang, S. Cao, S. Singamaneni, *Acc. Chem. Res.* **2019**, *52*, 1215.
- [198] H. Zhang, P. Tang, Y. Tang, C. Sun, K. Yang, W. Feng, Q. Wang, *Langmuir* **2023**, *39*, 7345.
- [199] N. S. Fuzil, N. H. Othman, N. H. Alias, F. Marpani, M. H. D. Othman, A. F. Ismail, W. J. Lau, K. Li, T. D. Kusworo, I. Ichinose, M. M. A. Shirazi, *Desalination* **2021**, *517*, 115259.
- [200] Y. Guo, H. Lu, F. Zhao, X. Zhou, W. Shi, G. Yu, *Adv. Mater.* **2020**, *32*, 1907061.
- [201] P. Liu, Y. B. Hu, X. Y. Li, L. Xu, C. Chen, B. Yuan, M. L. Fu, *Angew. Chem., Int. Ed.* **2022**, *61*, 202208587.
- [202] Z.-Y. Wang, L. Xu, C.-H. Liu, S.-J. Han, M.-L. Fu, B. Yuan, *J. Mater. Chem. A* **2024**, *12*, 10991.
- [203] B. Peng, Y. Gao, Q. Lyu, Z. Xie, M. Li, L. Zhang, J. Zhu, *ACS Appl. Mater. Interfaces* **2021**, *13*, 37724.
- [204] Q. Zhao, Y. Yang, B. Zhu, Z. Sha, H. Zhu, Z. Wu, F. Nawaz, Y. Wei, L. Luo, W. Que, *Desalination* **2023**, *568*, 116999.
- [205] X. Zhou, Y. Guo, F. Zhao, G. Yu, *Acc. Chem. Res.* **2019**, *52*, 3244.
- [206] N. An, R. Su, Z. Wang, W. Chen, W. Zhou, Q. Li, *Desalination* **2023**, *565*, 116849.
- [207] C. Pornrungrroj, A. B. Mohamad Annuar, Q. Wang, M. Rahaman, S. Bhattacharjee, V. Andrei, E. Reisner, *Nat. Water* **2023**, *1*, 952.
- [208] T. Zhang, F. Meng, M. Gao, W. L. Ong, K. G. Haw, T. Ding, G. W. Ho, S. Kawi, *EcoMat* **2021**, *3*, e12152.
- [209] L. Han, J. Mao, A.-Q. Xie, Y. Liang, L. Zhu, S. Chen, *Sep. Purif. Technol.* **2023**, *309*, 123003.
- [210] J. He, T. M. Tritt, *Science* **2017**, *357*, eaak9997.
- [211] J. R. Sootsman, D. Y. Chung, M. G. Kanatzidis, *Angew. Chem., Int. Ed.* **2009**, *48*, 8616.
- [212] L. Zhu, T. Ding, M. Gao, C. K. N. Peh, G. W. Ho, *Adv. Energy Mater.* **2019**, *9*, 1900250.
- [213] L. Chen, J. Ren, J. Gong, J. Qu, R. Niu, *Chem. Eng. J.* **2023**, *454*, 140383.
- [214] Z. Lin, T. Wu, Y.-F. Feng, J. Shi, B. Zhou, C. Zhu, Y. Wang, R. Liang, M. Mizuno, *ACS Appl. Mater. Interfaces* **2022**, *14*, 1034.
- [215] H. Li, S. Wang, Z. Yan, X. Niu, X. Sun, W. Hong, *Appl. Therm. Eng.* **2022**, *208*, 118279.
- [216] A. Ghaffar, Q. Imran, M. Hassan, M. Usman, M. U. Khan, *J. Environ. Chem. Eng.* **2022**, *10*, 108424.
- [217] J. Duan, B. Yu, L. Huang, B. Hu, M. Xu, G. Feng, J. Zhou, *Joule* **2021**, *5*, 768.
- [218] J. Shen, C. Yang, Y. Ma, M. Cao, Z. Gao, S. Wang, J. Li, S. Liu, Z. Chen, S. Li, *EcoMat* **2024**, *6*, e12428.
- [219] Z. Sun, C. Han, S. Gao, Z. Li, M. Jing, H. Yu, Z. Wang, *Nat. Commun.* **2022**, *13*, 5077.
- [220] T. Ding, K. Liu, J. Li, G. Xue, Q. Chen, L. Huang, B. Hu, J. Zhou, *Adv. Funct. Mater.* **2017**, *27*, 1700551.
- [221] G. Xue, Y. Xu, T. Ding, J. Li, J. Yin, W. Fei, Y. Cao, J. Yu, L. Yuan, L. Gong, J. Chen, S. Deng, J. Zhou, W. Guo, *Nat. Nanotechnol.* **2017**, *12*, 317.
- [222] L. Li, S. Feng, L. Du, Y. Wang, C. Ge, X. Yang, Y. Wu, M. Liu, S. Wang, Y. Bai, F. Sun, T. Zhang, *Nano Energy* **2022**, *99*, 107356.
- [223] A. Siria, M.-L. Bocquet, L. Bocquet, *Nat. Rev. Chem.* **2017**, *1*, 0091.
- [224] B. E. Logan, M. Elimelech, *Nature* **2012**, *488*, 313.
- [225] P. Yang, K. Liu, Q. Chen, J. Li, J. Duan, G. Xue, Z. Xu, W. Xie, J. Zhou, *Energy Environ. Sci.* **2017**, *10*, 1923.
- [226] J. Pu, H. Zhu, Q. Wang, Z. Qu, J. Zhang, *ACS Energy Lett.* **2024**, *9*, 2410.
- [227] B. Zhu, Z. Liu, Y. Peng, D. K. Macharia, N. Yu, M. Zhu, Z. Chen, *Nano Energy* **2023**, *117*, 108844.
- [228] H. He, X.-M. Song, M. Huang, X. Hou, Z. Song, Y. Zhang, *Green Chem.* **2023**, *25*, 9343.
- [229] C. Zhu, L. Xu, Y. Liu, J. Liu, J. Wang, H. Sun, Y.-Q. Lan, C. Wang, *Nat. Commun.* **2024**, *15*, 4213.
- [230] J. Lao, S. Wu, J. Gao, A. Dong, G. Li, J. Luo, *Nano Energy* **2020**, *70*, 104481.
- [231] L. Zhu, M. Gao, C. K. N. Peh, X. Wang, G. W. Ho, *Adv. Energy Mater.* **2018**, *8*, 1702149.
- [232] M. Gao, C. K. Peh, H. T. Phan, L. Zhu, G. W. Ho, *Adv. Energy Mater.* **2018**, *8*, 1800711.
- [233] L. Li, S. Feng, Y. Bai, X. Yang, M. Liu, M. Hao, S. Wang, Y. Wu, F. Sun, Z. Liu, T. Zhang, *Nat. Commun.* **2022**, *13*, 1043.
- [234] H. Wang, W. Xie, B. Yu, B. Qi, R. Liu, X. Zhuang, S. Liu, P. Liu, J. Duan, J. Zhou, *Adv. Energy Mater.* **2021**, *11*, 2100481.
- [235] H. He, Z. Song, Y. Lan, M. Huang, S. Wu, C. Ben, D. He, X. Hou, X.-M. Song, Y. Zhang, *ACS Appl. Mater. Interfaces* **2023**, *15*, 17947.
- [236] X.-Q. Wang, G. W. Ho, *Mater. Today* **2022**, *53*, 197.
- [237] K. Wang, J. Ren, S. Yang, H. Wang, *Adv. Mater. Technol.* **2021**, *6*, 2100158.
- [238] X.-Q. Wang, C. F. Tan, K. H. Chan, X. Lu, L. Zhu, S.-W. Kim, G. W. Ho, *Nat. Commun.* **2018**, *9*, 3438.
- [239] X.-Q. Wang, K. H. Chan, Y. Cheng, T. Ding, T. Li, S. Achavananthadith, S. Ahmet, J. S. Ho, G. W. Ho, *Adv. Mater.* **2020**, *32*, 2000351.
- [240] Q. Shi, H. Xia, P. Li, Y.-S. Wang, L. Wang, S.-X. Li, G. Wang, C. Lv, L.-G. Niu, H.-B. Sun, *Adv. Opt. Mater.* **2017**, *5*, 1700442.
- [241] Y. Cao, W. Li, F. Quan, Y. Xia, Z. Xiong, *Front. Mater.* **2022**, *9*, 827608.
- [242] X. Cui, Z. Liu, B. Zhang, X. Tang, F. Fan, Y. Fu, J. Zhang, T. Wang, F. Meng, *Chem. Eng. J.* **2023**, *467*, 143515.
- [243] Y. Zheng, C. Li, *Giant* **2023**, *16*, 100192.
- [244] D. Pan, D. Wu, P.-J. Li, S.-Y. Ji, X. Nie, S.-Y. Fan, G.-Y. Chen, C.-C. Zhang, C. Xin, B. Xu, S. Zhu, Z. Cai, Y. Hu, J. Li, J. Chu, *Adv. Funct. Mater.* **2021**, *31*, 2009386.
- [245] B. Wang, J.-H. Wang, Q. Liu, H. Huang, M. Chen, K. Li, C. Li, X.-F. Yu, P. K. Chu, *Biomaterials* **2014**, *35*, 1954.
- [246] Q. Ren, B. Li, Z. Peng, G. He, W. Zhang, G. Guan, X. Huang, Z. Xiao, L. Liao, Y. Pan, X. Yang, R. Zou, J. Hu, *New J. Chem.* **2016**, *40*, 4464.
- [247] Z. Sun, H. Xie, S. Tang, X.-F. Yu, Z. Guo, J. Shao, H. Zhang, H. Huang, H. Wang, P. K. Chu, *Angew. Chem., Int. Ed.* **2015**, *54*, 11526.
- [248] Y. Wang, Y. Dong, F. Ji, J. Zhu, P. Ma, H. Su, P. Chen, X. Feng, W. Du, B.-F. Liu, *Sens. Actuators, B* **2021**, *347*, 130613.
- [249] S. Watanabe, K. Arikawa, M. Uda, S. Fujii, M. Kunitake, *Langmuir* **2021**, *37*, 14597.



**Wei Li Ong** received his B.Eng. (Hons.) and Ph.D. degrees from the National University of Singapore (NUS) in 2008 and 2012, respectively. He is currently a Research Fellow at the Department of Electrical and Computer Engineering at NUS. His research interests primarily focus on nanomaterials for clean energy generation, photocatalytic water splitting, and atmospheric water harvesting.



**Wanheng Lu** received her Ph.D. degree from the National University of Singapore (NUS) in 2017. She is currently a Research Fellow at the Department of Electrical and Computer Engineering at NUS. Her research interests include nanomaterials and functional materials for energy and water generation, and multidimensional characterization of materials under multiple fields based on scanning probe microscopy (SPM) techniques.



**Tianxi Zhang** received her Ph.D. degree in chemical and biomolecular engineering from the National University of Singapore (NUS) in 2023. Currently, she is a Research Fellow at the Department of Electrical and Computer Engineering at NUS. Her research interests are mainly focused on the utilization of solar energy for hydrogen production, carbon dioxide reduction, and photoassisted catalysis.



**Ghim Wei Ho** received her Ph.D. degree in semiconductor nanostructures from the Nanoscience Centre, University of Cambridge in 2006. She is a Professor of the Department of Electrical and Computer Engineering, the National University of Singapore (NUS). She leads the Sustainable Smart Solar System research group working on fundamental and applied research on nanosystems with emerging low-dimensional nanomaterials, interfacial interactions, and hybridized functionalities for energy, environment, electronics, and healthcare.